**LANCASTER UNIVERSITY**

# Effective Mechanism and the Source Region of the Stimulated ELF/VLF Waves by High Power HF Radio Waves

by

Zhe Guo

A thesis submitted in partial fulfilment for the degree of MSc by Research

in the
Faculty of Science and Technology
Department of Physics

Sep 2020

# Declaration of Authorship

I, Zhe Guo, declare that this thesis titled, *'Effective Mechanism and the Source Region of the Stimulated ELF/VLF Waves by High Power HF Radio Waves'* and the work presented in it are my own. I confirm that:

- This work was done wholly or mainly while in candidature for a research degree at this University.
- Where any part of this thesis has previously been submitted for a degree or any other qualification at this University or any other institution, this has been clearly stated.
- Where I have consulted the published work of others, this is always clearly attributed.
- Where I have quoted from the work of others, the source is always given. With the exception of such quotations, this thesis is entirely my own work.
- I have acknowledged all main sources of help.
- Where the thesis is based on work done by myself jointly with others, I have made clear exactly what was done by others and what I have contributed myself.
- The word length of this thesis is 18188 words (excluding the bibliography), which does not exceed the permitted maximum (35000 words).
- I grant the institutional repository of Lancaster University required permissions and conditions with respect to online access to my work.

Signed: _____

Date: _____

# Abstract

The ionosphere can be utilized as a natural plasma laboratory for the investigation of many nonlinear plasma processes by means of high-power, high-frequency radio waves, a process known as ionospheric heating.

One of the most important effects of ionospheric heating by High Frequency (HF) waves, is the generation of ELF/VLF (extremely low frequency/very low frequency) waves by modulated heating. This area of research has been a focus of many investigations for almost fifty years since the most basic method of amplitude modulation was proposed.

This dissertation introduces the main mechanisms of ionospheric heating as well as amplitude modulation and beat wave modulation in both D and F regions. An important limitation of amplitude modulation is its dependence on the ionospheric electrojet, which means in order to achieve better modulation effects, some strict spatio-temporal conditions must be met. In order to solve this problem, some possible methods have been proposed including beat wave modulation. However, due to the controversy of its mechanism and the source region of the stimulated ELF/VLF waves, it is not clear whether it is an electrojet-independent method or not, which has become one of the hot topics in recent years. This dissertation is focused on the identification of the mechanism and source region of beat wave modulation by means of constructing and simulation of physical models. The results are then compared to several observations reported in the literature in order to verify the validity of the proposed physical models.

# Arrangement of this dissertation

**Chapter 1: Introduction**

Literature review on the mechanism and research progress of ionospheric heating as well as modulated heating. In addition, the controversy of different theories about beat wave modulation is introduced.

**Chapter 2: Numerical Model of Ionospheric Heating**

Based on different mechanisms (mainly the transport process), models of ionospheric heating in D-E region and F region are established respectively.

**Chapter 3: Numerical Model of Amplitude Modulation and Beat Wave Modulation**

As the fundamental technique of modulated heating, the mechanism of amplitude modulation as well as some simulation results compared with references are introduced. As a contrast, the mechanism and characteristics of beat wave modulation are introduced, some simulation results compared with references are introduced.

**Chapter 4: Identification of Mechanism and Source of Beat Wave Modulation**

A new method to identify the source region for the beat wave modulation is proposed by combining the preheating technique.

**Chapter 5: Summary and Prospect**

This chapter summaries the results and suggest future investigations.

# Acknowledgement

The unusual 2020 has been half passed and my post graduate year is also coming to an end. Reviewing my past year at Lancaster University, I see happiness and confusion, but more importantly, gratefulness. I am grateful to everyone who stood by me and helped me.

Firstly, I would like to express my gratitude to my supervisor Prof. Farideh Honary. Prof. Farideh Honary guided me like a beacon in the ocean of study and led me into the research in this field. She gave me much support, guidance and suggestions during my research. Without her, I could not have completed this dissertation.

I am also grateful to Prof. Jun Wu and Prof. Chen Zhou, who supported me and gave me much advice when I was lost. I became firm about my study in the U.K., thanks to them.

Besides, I would like to express my heartfelt thanks to all staff of Graduate College at Lancaster University. They offered a comfortable environment for my college life so that I felt being cared even tens of thousands of miles away from home.

Finally and most importantly, I would like to express my gratitude to my parents who are always my powerful backing. They supported my every choice with all they have so I can complete my study without concern.

# Contents

# List of Figures

# List of Tables

# Chapter 1

# Introduction

## 1.1 Introduction of the ionosphere

The part of the upper atmosphere ionized by ultraviolet and X-ray radiation from the sun is the Earth's ionosphere. It starts from 60 km and extends to 1000 km altitude. According to IRE (Institute of Radio Engineers), there are plenty of free electrons (but much less than neutral density) in the ionosphere so that they can affect the transmission of radio waves.

Essentially, the ionosphere is a sort of plasma formed by ionization of solar radiation, and it is quasi-neutral on macro-scale. In addition, the whole ionosphere is in the geomagnetic field, so it is also a weakly ionized magnetic plasma. The ionosphere consists of neutral gases as well as ionized electrons and ions, which are involved in many kinetics, electrodynamics, thermodynamics and photochemical reactions. The main characteristic parameters of the ionosphere include ion composition and corresponding density and temperature, electron density and temperature, neutral particle composition and corresponding density and temperature, collision frequency between different components, plasma frequency, etc. Among these particles, electrons can reflect ionospheric characteristics better because electrons not only reflect the level of ionization as an important criterion of distinguishing the layers of the ionosphere, but also significantly impact navigation and communication by

affecting the transmission of radio waves. Therefore, more attention is paid to electrons in the study of ionospheric characteristics, as a result, electrons are often the main object to monitor and measure ionospheric evolution.

The ionosphere has an obvious stratification structure, the composition, content and profile of neutral gases and ion, as well as electron density, are quite different in different altitude layers. The lower ionosphere is in photochemical equilibrium and the upper ionosphere is in diffusion equilibrium. According to the characteristics of ion distribution, the ionosphere can be divided into D, E and F layer (F layer can also be subdivided into F1 and F2 layers in the daytime). The ingredient of D layer at a height of 60~90 km is mainly a multi-atomic ion group and negative ions, but the ionization level is very low, the electron density is about $10^2$~$10^4$/cm$^3$ in this region; the height of E layer (also known as generator layer) is about 90~140 km, the main components are molecular ions ($NO^+$, $O_2^+$), the electron density is about $10^3$~$10^5$/cm$^3$; the F layer is the dense region of atomic ions ($O^+$), the electron density is about $10^5$~$10^6$/cm$^3$, the F1 layer is within the height range of 140~220 km, it is the transition zone between molecular ion layer and atomic ion layer, so it has obvious diurnal variation characteristics. After sunset, it disappears due to the rapid recombination of electrons and ions, the region above 220 km corresponding to $O^+$ peak is the F2 layer, the peak of electron density is also located here. The plasma frequency corresponding to the peak of electron density is called F2 layer critical frequency. The region above the F layer is the top ionosphere, which contains low density $H^+$ and $He^+$, so it is also called the proton layer (Xiong et al., 1999; Wang and Lv, 2012). The stratification structure of the ionosphere and the electron density in each layer are shown in Figure 1.1 (Gurevich, 2007).

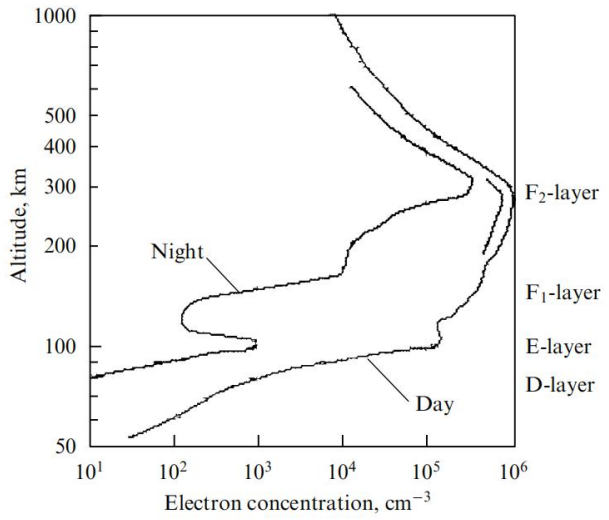


Figure 1.1 Altitude distribution of electron density in different ionospheric layer and different time of day (from Gurevich, 2007).

The electron density in the ionosphere has not only spatial characteristics of varying with height, latitude and longitude, but also temporal characteristics of varying with diurnal variation, sunspot cycle and seasonal variation. In addition, there are many "abnormal" phenomena, such as winter absorption anomaly in the D layer and additional stratification of the F1 layer during solar eclipse period. The ionosphere is also affected by the lower atmosphere, such as the TID (travelling ionospheric disturbance) in the F layer generated by the upward transmission of energy of atmospheric gravity waves generated by the combined action of gravity and thermal pressure (as shown in Figure 1.2).

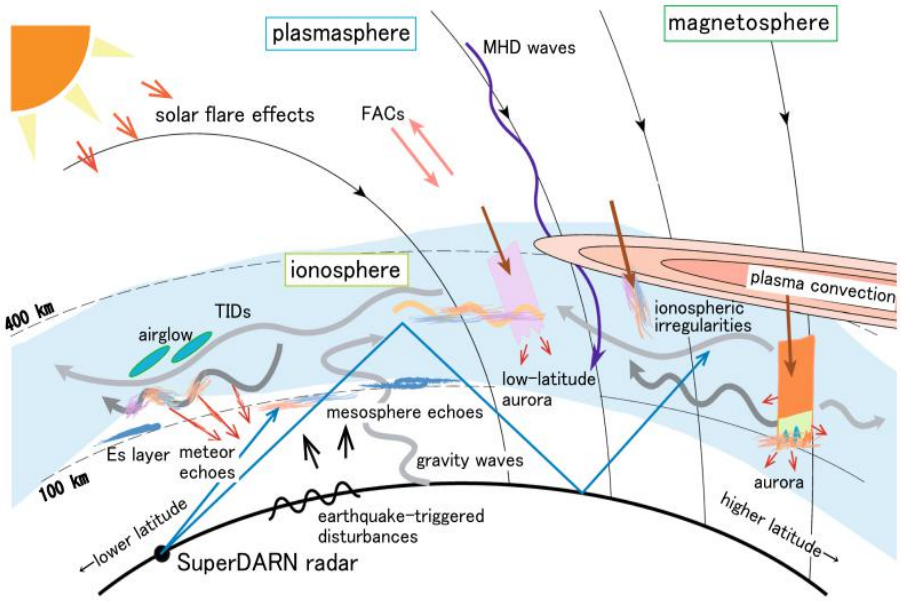


Figure 1.2 Some natural phenomena in the ionosphere (from Nishitani et al., 2019)

## 1.2 Introduction of ionospheric heating

With the development of science and technology, the relationship between the ionosphere and humans is getting closer and closer. One of the important methods for understanding the ionospheric environment is ionospheric heating by high frequency radio waves. This mechanism is significant in the following aspects: firstly, the ionosphere can be used as a natural plasma laboratory, research on ionospheric heating is helpful for humans to deepen the understanding of the plasma characteristics. Furthermore, due to the importance of the ionospheric environment for shortwave communication, over-the-horizon radar, aerospace, etc, the requirements of its application has also contributed to the development of ionospheric heating.

The history of the ionosphere is short, it was not widely known until 1901 when Marconi completed the famous experiment with radio waves transmission across the Atlantic. This landmark experiment in the history of communication immediately made people realize the importance of the ionosphere for radio communication, on the other hand, it has been realized that the quality of radio communications was highly

constrained by the ionospheric condition. On this basis, the Luxembourg effect discovered by Tellegen in 1933 became the beginning of the research of nonlinear effects and HF heating in the ionosphere (Tellegen, 1933).

During nearly 90 years since the discovery of "Luxembourg effect", great progress has been made in the study of ionospheric modification. As one of the main influencing methods, ionospheric heating by high-frequency radio waves has been paid more and more attention. The research process is mainly divided into two stages: the first stage is from the 1930s to 1960s, which is the stage of theoretical research. During this period, in 1937, Bailey first proposed the idea of artificially increasing the ionization level of the ionosphere by emitting high-power radio waves (Bailey, 1937a); after that, in 1938, he came up with the idea of lighting up the night sky with artificially stimulated electron cyclotron heating in the E region (Bailey, 1937b). Based on the previous theoretical research, in consideration of the importance of the ionosphere for radio wave propagation, the idea of creating a more favorable environment for the propagation of radio waves by exciting electron cyclotron heating and disturbing electron density in the local ionosphere using powerful HF waves was proposed (Bailey and Goldstein, 1958). This is the beginning of research on modifying the ionospheric environment by artificial technique. In 1960, Ginzburg and Gurevich proposed the idea of artificial modification of the ionosphere by powerful HF waves in the F region (Ginzburg and Gurevich, 1960). The second stage is from the 1960s to the present. On the basis of previous theoretical research, in the late 1960s, the first experimental device dedicated to ionospheric heating (called heater) in the world was built on Platteville, Colorado, which meant that more scientific methods were employed for research on ionospheric heating by high-power high-frequency radio waves. This heater utilized a continuous-wave transmitter, with a maximum radiated power of 2 MW, the range of transmitting frequency was 2.7-25 MHz, with the gain of the antenna of 19 dbi (Utlaut and Cohen, 1971). Many theoretical research results and conjectures about ionospheric heating have been verified after this device was put into operation, such as increasing local electron density and electron temperature (Utlaut

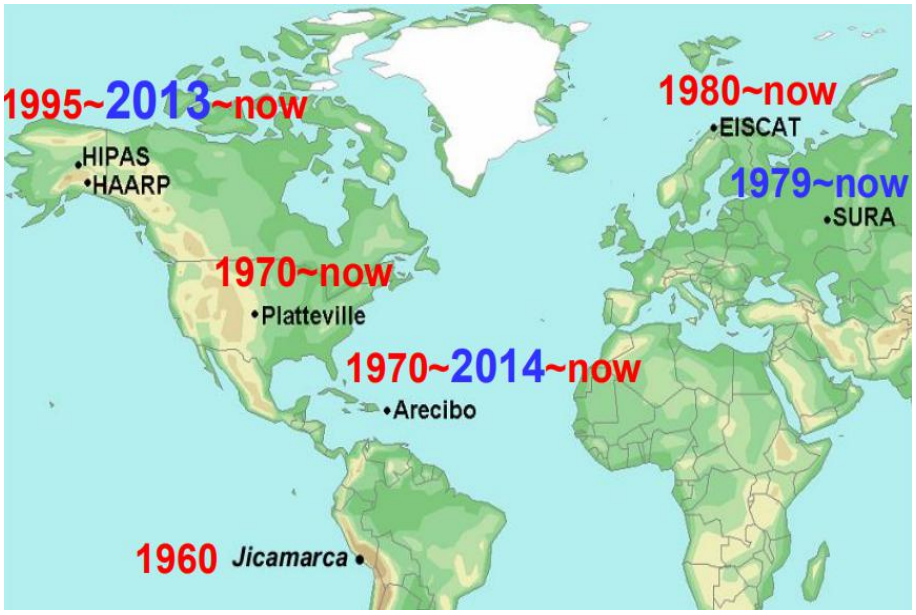


Figure 1.3 Map of HF ionospheric heating facilities, the date of each facility represents when the heater was built or when the upgrade was completed (from Fu, 2017)

| Device | Platteville | Arecibo | SURA | Tromsø | HIPAS | HAARP |
|---|---|---|---|---|---|---|
| Year of first experiment | 1970 | 1980 | 1980 | 1980.9 | 1977 | 1997 |
| Latitude | 40.18°N | 18°N | 56.13°N | 69.6°N | 64.91°N | 62.39°N |
| Longitude | 104.73°W | 67°W | 46.1°E | 19.2°E | 146.83°W | 145.15°W |
| Geomagnetic latitude | 49° | 32° | 71° | 67° | 65° | 62° |
| Power (MW) | 1.6 | 0.8 | 0.75 | 1.5 | 1.8 | 3.6 |
| Range of frequency (MHz) | 2.7~25 | 3~15 | 4.5~9 | 3.8~8 | 2.8~4.5 | 2.8~10 |
| Gain (dB) | 18 | 25 | 26 | 28 | 19 | 30 |
| ERP (MW) | 200 | 300 | 400 | 1200 | 120 | 3000 |

Table 1.1 Parameters of major international ground-based ionospheric heating devices

and Violette, 1972), forming artificial Spread-F (Allen et al., 1974) as well as FAI

(field-aligned irregularity) (Thome and Blood, 1974) and so on. After that, several heaters were built and put into operation around the world, more and more significant experiments were carried out. The map and parameters of several major international ground-based ionospheric heating devices are shown in Figure 1.3 and Table 1.1 (Li, 2006).

As shown in Table 1.1, most of these heaters are located in mid and high latitudes except Arecibo (Rietveld, 2003; Frolov et al., 2008). A vast amount of experimental investigations have been carried out in the last five decades. These investigations have reported interesting nonlinear processes mainly in the F and E regions due to the interaction of powerful HF radio waves with ionospheric plasma. Experiments at SURA facility between 1980-1996, have revealed the characteristics of SSI (small-scale irregularity) generated by ionospheric heating at the height of F layer (Frolov et al., 1997); the ELF/VLF waves generated by modulated heating on HAARP during 100 days were extensively studied (Cohen and Golkowski, 2013); generation of artificial airglow at 630.0 nm at Tromsø was first reported in the ionospheric heating experiments on February 1999 (Sergienko et al., 2000; Kosch et al., 2000), subsequently, artificial airglow at 630.0 nm was detected at HAARP for the first time in March 1999 (Pedersen et al., 2001).

A common feature in all heating experiments is the disturbance in ionospheric plasma, such that there always be a region with a decrease of electron density and several regions with an increase of electron density along the magnetic field (Duncan et al., 1988; Bernhardt et al., 1989; Milikh et al., 2010a); these effects can reach up to the magnetosphere (Perrine et al., 2006; Carpenter, 2002). Distribution of electron density along the magnetic field and its vertical direction can profoundly influence the propagation of radio waves: when the electron density gradient perpendicular to the magnetic field is sufficient to bring the total reflection of VLF/ELF waves, and a waveguide tube along the magnetic field for propagation of VLF/ELF waves is formed (Streltsov et al., 2006). This is supported by relevant research based on a VLF

transmitter (Siple Station, Antarctica) (Helliwell, 1988) and the HAARP HF heater (Inan, 2004).

Although these heating experiments enrich our understanding of the ionospheric effect, they are associated with a large amount of costs (Fejer et al., 1985). Therefore, computer numerical simulation is important, especially for quantitative evaluation of some experiments which are difficult to carry out. Meltz et al. (1982) simulated the perturbation of electron temperature and density in the magnetic meridian plane caused by O-mode wave in an overdense heating experiment. O-mode (ordinary mode) wave, i.e., left-hand circularly polarized wave, which means circular polarization of an electromagnetic wave in which the electric field vector rotates in a counterclockwise direction, as seen by an observer looking in the direction of propagation of the wave (Weik, 2000a). X-mode (extraordinary mode) wave, i.e., right-hand circularly polarized wave, which means circular polarization of an electromagnetic wave in which (a) the electric field vector rotates in a clockwise direction as the wave advances in the direction of propagation and as seen by an observer looking in the direction of propagation and (b) in a waveguide, the electric field vector always remains perpendicular to the direction of propagation as well as perpendicular to the magnetic field vector (Weik, 2000b). When the heating wave is vertical to the ionosphere, it will propagate upward when its frequency is greater than ionospheric plasma frequency and will reflect when its frequency is less than ionospheric plasma frequency. Therefore, during the process of ionospheric heating, when the frequency of HF wave is greater than the ionospheric plasma frequency in a layer, it is called underdense heating, while when the frequency of HF wave is less than the ionospheric plasma frequency in a layer, it is called overdense heating. In the case of overdense heating, the reflection heights of O/X wave correspond to their respective cutoff frequency, the reflection height of X wave is slightly lower than that of O wave, characteristic trajectories of O/X wave reflection are shown in Figure 1.4 (Gurevich, 2007). In upper hybrid height, $f_0^2 = f_{pe}^2 + f_{ce}^2$, where $f_0$ is the frequency of the

electromagnetic wave, $f_{pe}$ is the plasma frequency, $f_{ce}$ is the electron gyrofrequency (Vartanyan et al., 2016). HF waves can stimulate Langmuir parametric instability, including parametric decay instability and oscillating two-stream instability, at O wave reflection height. At the upper hybrid height, HF waves can stimulate thermal parametric instability, including thermal oscillating two-stream instability and thermal parametric decay instability (Zhou et al., 2018), meanwhile, HF waves excite the high frequency and low frequency plasma waves at the corresponding height through the parametric coupling process above. Based on Maxwell's equations and MHD (magnetohydrodynamics) fundamental equations, in consideration of thermal self-focusing effect, the governing equations of ionospheric heating by powerful HF waves have been established, the spatio-temporal evolution process of plasma parameters during the heating has been simulated by Bernhardt and Duncan (1982). In 1992, the Hansen boundary condition was proposed, which has been widely used in the numerical simulation (Hansen et al., 1992). In the same year, a self-consistent Ohmic heating model considering the ionospheric transport process and the propagation path of radio waves was established by Hinkel-Lipsker et al. (1993). Considering the non-uniform distribution of gradient in the ionospheric plasma and the distribution of the transport coefficient with height, the results of ionospheric heating of both E and F layer in the mid-latitude area were simulated (Blaunstein, 1996).

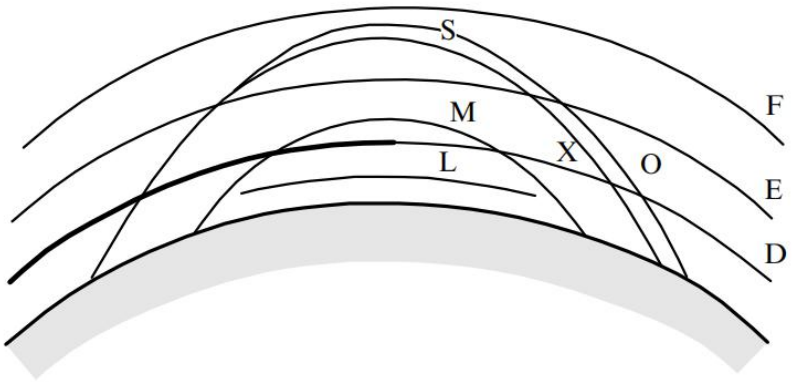


Figure 1.4 Characteristic trajectories of O/X wave reflection. S, M, L represent Short waves, Medium waves and Long waves respectively. D, E, F represent different ionospheric layer (from Gurevich, 2007).

Furthermore, the establishment of the ionospheric physical model gave a new idea for numerical simulation research. For example, in recent years, a series of ionospheric heating simulation have been carried out using SAMI2 (Sami2 is another model of the ionosphere) (Huba et al., 2000) and SAMI3 (Sami3 is also a model of the ionosphere) (Huba et al., 2008) models for research of artificial ionospheric duct (Perrine et al., 2006; Milikh et al., 2010b) and conjugate heating effects (Wu et al., 2012). By introducing the heating term into the electron energy equation, the SAMI2 model was used to make a two-dimensional simulation of ionospheric heating, the changes of field-aligned electron temperature and electron density were obtained, the results were highly consistent with the measured data (Milikh et al., 2008, 2010b, 2012). The effect of ionospheric heating near Arecibo (with low magnetic latitude) at the conjugate point under different background ionosphere conditions were simulated and analyzed by Wu et al. (2012), it was pointed out that better heating effect can be obtained with lower background electron density. In 2013, a three-dimensional simulation of ionospheric heating was carried out using the SAMI3/ESF (equatorial spread F) model, which mainly focused on the influence of E × B drift widely existing in the background ionosphere on the heating effect (Zawdie et al., 2013).

With the continuous upgrading of heating equipment and the development of computer technology, more valuable research results of ionospheric heating are expected in the future.

## 1.3 Introduction of ULF/ELF/VLF waves generated by modulated heating

ULF(3-30Hz)/ELF(30-3000Hz)/VLF(3-30kHz) waves are important not only for the navigation, communication and detection of underground targets, but also for the precipitation of energetic electron by wave-particle interaction in the radiation belts in order to protect the astronauts and spacecrafts in these regions. In addition, recently,

potential diagnostic methods for the D region by Amplitude Modulation (AM) of electrojet and its improved method have been proposed as a new application (Agrawal and Moore., 2012; Gołkowski et al., 2013; Maxworth et al., 2015). However, it is very hard to build and maintain a ULF/ELF/VLF antenna array because it requires a very large area. For example, the US Navy's VLF antenna (as shown in Figure 1.5) consists of 26 towers, the height of each of them is 850 to 1000 ft, the power of 18 MW consumed by the antenna is from a dedicated power plant (Nagaraja and Prasad., 2017). As a result, alternate methods are in demand.

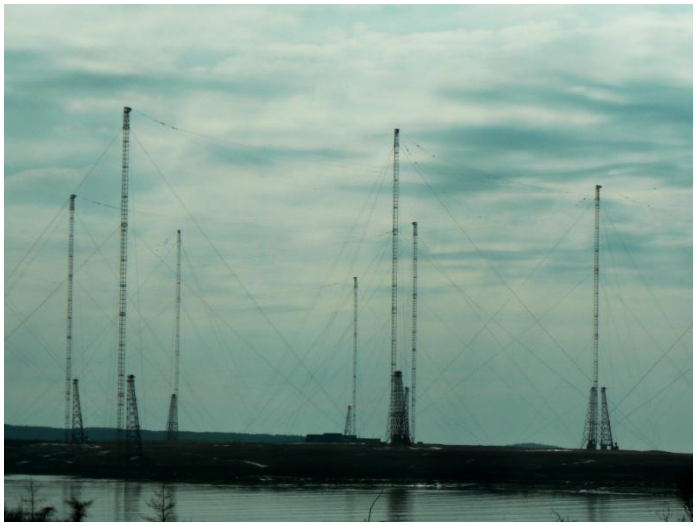

Figure 1.5 VLF antenna of US Navy (from Nagaraja and Prasad, 2017).

After decades of research, generating ULF/ELF/VLF waves by ionospheric modulated heating using powerful HF waves has been proved a reliable method. This idea was first proposed by Willis and Davis (1973), and was soon tested successfully for the first time by Getmantsev et al. (1974). Its basic principle is: the high-frequency heater is switched on and off with the frequency of the desired ULF/ELF/VLF waves, giving rise to increases and decreases of local electron temperature with the modulation frequency. Such periodic changes in electron temperature will cause corresponding changes in electron density and conductivity, generating the modulation current. When there is an electrojet in the ionosphere, the modulated current will enhance the current and radiate the low-frequency signal. This method is called Amplitude Modulation (AM). The emergence of AM gives people a new perspective, on this basis, scientists

have carried out numerous theoretical investigations and experiments in Russia, Europe and the United States for decades (Streltsov et al., 2018).

But both theoretical and experimental investigations show that the efficiency of amplitude modulation is very low. Moore et al. (2007) carried out experiments at HAARP which adopted sinusoidal amplitude modulation to generate 2125 Hz ELF waves and found the transformation efficiency (HF to ELF) is only ~0.0004 – 0.0032%. In addition, Stubbe et al. (1985) pointed out that amplitude modulation can only be used for generating waves whose frequency is less than 23 kHz. Therefore, improving the generation efficiency and expanding the frequency range of generated low-frequency waves have been the focus of research.

On the basis of traditional amplitude modulation, Rietveld et al. (1986) established the theoretical model by combining experiments and pointed out that the electron heating time constant is shorter than the electron cooling time constant when modulating the Hall conductivity in the D region. Papadopoulos et al. (1990) proposed two methods to improve the efficiency of AM: 1) sweeping the antenna beam over an area on a time scale faster than the cooling rate at the heating altitude, which is an application of the difference between electron heating time constant and electron cooling time constant mentioned above; 2) modulating the Pederson conductivity at the E region (90-100 km). Cohen et al. (2012) found that the efficiency of AM decreases with the increase of the incident HF wave frequency and increases with the increase of the heating area, which was verified by experiments in HAARP. Yang et al. (2019a) pointed out that AM with X wave is more efficient than O wave; in order to obtain better ELF/VLF generation, the optimal frequency of HF waves is found to be 0.8~0.9 and 0.75~0.85 times of $f_oE$ for O wave and X wave, respectively.

# 1.4 Mechanisms of Modulating ULF/ELF/VLF Waves

In general, the methods of modulating low frequency waves can be divided into several categories as described below:

## 1.4.1 Improved Methods Based on Traditional Amplitude Modulation

### 1.4.1.1 Beam Painting

Beam Painting (BP) was proposed by Papadopoulos et al. (1989) (cited in Cohen et al., 2010a). The idea here is that the time constants of electron heating and cooling in the ionosphere caused by switching on and off the heater are different and in most cases, the heating time constant is much less than the cooling time constant (Rietveld et al., 1986), the narrow beam HF waves are therefore made to heat each point in the larger ionospheric region that is expected to be heated at a heating time constant, then the HF beam will be moved quickly to the next point and return to the first point before it cools completely (that is, t < cooling constant time). Therefore, this method can effectively expand the heating area so that to achieve the purpose of improving the modulation efficiency, which means that the key of BP is that the heating time constant is much smaller than the cooling time constant. Barr et al. (1999) studied the modulation efficiency of BP and found that the source of the fundamental frequency and odd harmonics waves are in the higher ionospheric altitude, where the heating time constant is approximate to the cooling time constant, so the modulation efficiency of BP is not significantly improved compared with AM, on the other hand, the source of even harmonics waves is in lower ionospheric altitude, where the heating time constant is more than an order of magnitude less than the cooling time constant, so BP can significantly improve the modulation efficiency in the lower ionospheric altitude. In addition, the modulation efficiency and characteristics of amplitude modulation, beam painting and geometric modulation are compared by Cohen et al. (2010a, 2010b) as well as Robinson and Moore (2017), which will be introduced in section 1.4.1.2.

#### 1.4.1.2 Geometric Modulation

Cohen et al. (2008) reported a method called geometric modulation (GM), this method based on controlling the incidence direction of HF wave, make the HF beam scan the ionosphere in certain geometric patterns (such as circle sweep, line sweep, sawtooth sweep and so on) to modulate the electrojet. Unlike BP, GM adopts continuous-wave (CW), the geometric motion of CW in space replaces the periodic on-off of the heater, the period in which a scan is completed matches the frequency of the modulated low frequency wave. On the basis of experiments in HAARP, Cohen et al. (2008) found that GM is less efficient than AM when the modulated frequency is lower than 2 kHz but significantly more efficient when the modulated frequency is higher than 3 kHz. In particular, the enhancement effect of GM compared to AM is more obvious (7-11 dB) for long distances. Furthermore, Cohen et al. (2008) also pointed out that GM has a level of directionality. For example, the low-frequency signals generated along the scanning direction were significantly stronger than those generated perpendicular to scanning direction under line sweep.

On the other hand, Moore and Rietveld (2009) illustrated that GM is essentially the oblique AM modulation mentioned by Barr et al. (1988). In response to this question, Cohen et al. (2009) explained the difference between GM and oblique AM modulation in terms of generation efficiency and geometric effects, argued that the mechanism of GM is close to the two-element phased array mentioned by Barr et al. (1987). Furthermore, it has been shown that GM is more complicated when utilizing new upgrade ability at HAARP. Therefore, Cohen et al. (2009) emphasized that GM is an “unprecedented technique”.

As mentioned in section 1.4.1.1, BP is also a technique for modulated heating by controlling the movement of HF beams, so Cohen et al. (2010a, 2010b) quantitatively compared AM, BP and GM through experiments and theoretical models and found that compared with AM, BP is suitable for modulating waves in a lower frequency range (such as ULF waves), and the enhancement of excitation is mainly concentrated

near the heating site; in contrast, GM can be more efficient at longer distances from the heating site. The characteristic "a level of directionality" of geometric modulation is also verified. Recently Robinson and Moore (2017) proposed a method called "optimized beam painting algorithm (OBP)" which changes the azimuth and zenith angles of the heater to construct a phased array of ELF/VLF source in the ionosphere, on the basis of experimental results of over 1200 times in HAARP, they believed that compared to vertical AM, oblique AM and GM, OBP can really increase the received signal amplitudes of ELF/VLF waves. The schematic comparison of AM, BP and GM is shown in Figure 1.6.

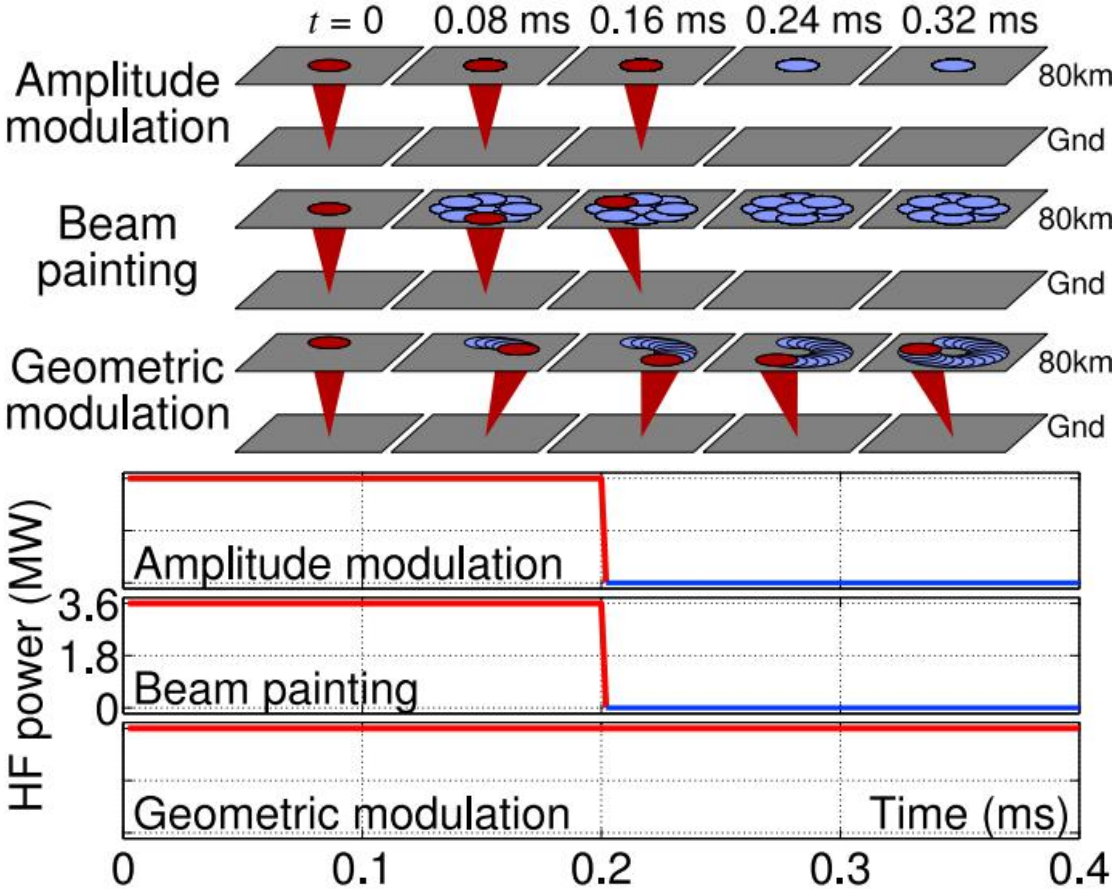


Figure 1.6 Schematic comparison of AM, BP and GM. (top) The progression of the HF beam at five points during a ELF/VLF period (which is 0.4 ms for f = 2.5 kHz). Bottom panel indicates the cases of AM and BP the HF transmitter is turned ON and OFF with a duty cycle of 50%. In GM case no power modulation is involved but instead the constant beam makes a slower sweep along a geometric shape, in this case a circle (from Cohen et al., 2010a).

#### 1.4.1.3 Pre-heating

Generation efficiency of ULF/ELF/VLF waves can be significantly improved by "preheating" the modulation region using HF waves before modulated heating, there are two reasons as follow: firstly, preheating reduces the electron-ion recombination coefficient, resulting in an increased electron density and current density in the ionosphere; secondly, preheating reduces low altitude self-absorption to sharpen the density profile which leads to more efficient heating. This method was proposed by Milikh and Papadopoulos (2007), who calculated that preheating could increase the signal intensity of low-frequency waves generated by modulated heating by up to 7 dB.

#### 1.4.1.4 Dual-Beam HF Modulation

Moore and Agrawal (2011) proposed a method using continuous-wave and HF wave modulated by ELF/VLF frequency simultaneously to generate corresponding ELF/VLF waves, this method is called Dual-Beam HF Modulation (as shown in Figure 1.7). The main difference between dual-beam HF modulation and beat wave modulation mentioned below is that the two sub-arrays of dual-beam modulation emit continuous wave and discontinuous wave modulated by ELF/VLF respectively and the carrier frequency of these two waves can be the same. Beat wave modulation, on the other hand, utilizes two continuous waves with a frequency difference of $f$ ($f$ is the ELF/VLF modulated frequency) transmitted by two sub-arrays (Kuo et al. 2012). On the basis of experiments in HAARP and the establishment of the theoretical model, Moore and Agrawal (2011) found that continuous-wave would lead to a decrease in modulation efficiency, so it is not a preferred way to generate ELF/VLF waves compared to AM. On the other hand, further analysis (Agrawal and Moore, 2012) pointed out that the intensity of ELF/VLF wave is sensitive to the altitude distribution of electron density and electron temperature at D region, so dual-beam modulation could be an applicable D-region diagnostic. Gołkowski et al. (2013) found that dual HF beams with AM (both of the two beams are modulated HF waves at ELF/VLF

with a phase offset) can also be a potential diagnostic method for the D region, although it may need experiments with finer and more rapid ELF phase stepping guided by comprehensive modeling.

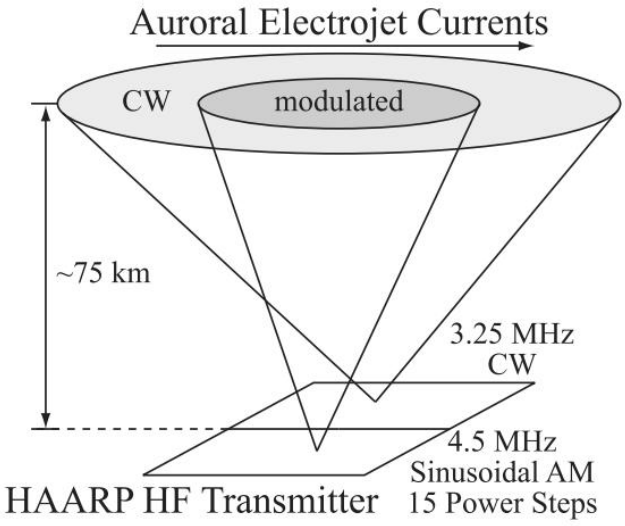


Figure 1.7 Schematic of dual-beam HF heating experiment. The 3.25 MHz CW beam is broader than the 4.5 MHz modulated beam (from Moore and Agrawal, 2011).

In addition, there are some other methods relevant to AM. Villaseñor et al. (1996) compared traditional AM with a method called demodulation mode (DM). The process of DM is to conduct vertical heating during the former half time of a modulation period, and then the beam is separated to heat regions on either side of the vertical position so that subdividing the array into two sub-arrays during the latter half time of a modulation period. The experimental results indicated that the intensity of ELF/VLF waves generated by DM is only about half of AM. Gołkowski et al. (2009) proposed that cross modulation could be used to generate waves in the range of 630 Hz~37 kHz, the intensity of ELF/VLF wave generated by this method is an order of magnitude weaker than AM, although it is able to produce waves with a wider frequency range than AM (>30 kHz). Furthermore, the author mentioned that the harmonics modulated by AM can also generate waves higher than 30 kHz with similar intensity to cross modulation.

The above methods can be classified as improvements to AM because they are essentially the same as AM, which changes electron temperature in the D region and lower E region periodically by switching on and off the heater or other equivalent methods that can achieve the same effect, thus inducing the periodic changes of conductivity and superimposing them on the electrojet to produce ELF/VLF waves.

In this context, it can be seen that the modulation efficiency of AM and its improved methods are inevitably affected by the strength of the background electrojet and the heating and cooling time constants. The heating time constant can usually be shortened by increasing the power of the heater, but the strength of electrojet in the background and cooling time constant are difficult to control artificially. The strength of electrojet limits the time and location of modulated heating: the electrojet in mid-latitude is weak in general, so AM is more suitable for modulated heating in the polar and the equatorial regions, but the polar electrojet does not exist all the time and is hard to predict, furthermore, there are not enough suitable facilities to carry out the experiments in the equatorial regions. In addition, as the frequency of modulation increases, the deficiency of cooling time will become more and more obvious, resulting in a serious attenuation of the signal strength (Kuo et al., 2010). Therefore, scientists have proposed some other modulation mechanisms that are independent or less dependent on the electrojet as well as the heating and cooling time.

### 1.4.2 Beat Wave Modulation

VLF, ELF and ULF waves can be modulated by using two separate heating arrays transmitting HF continuous waves whose frequencies are different from f (f is the frequency needs to be modulated) (Kotik et al., 1986, Noble and Gordon, 1990 cited in Barr and Stubbe, 1997), this mechanism is called beat wave modulation (BW). Villaseñor et al. (1996) pointed out that the low-frequency waves excited by AM are the strongest at almost all the modulated frequencies by comparing the excitation efficiency of low-frequency waves in various frequency segments generated by AM

and BW, although BW can produce a more stable low-frequency signal in some cases. In addition, the excitation efficiency of X-mode wave is higher than that of O-mode wave by a factor of two, either using AM or BW modulation. The experimental observations of Barr and Stubbe (1997) confirmed the conclusion of Villaseñor et al. (1996). Furthermore, Barr and Stubbe (1997) also pointed out that the modulation efficiency of BW might be higher than that of AM by adjusting the receiver position, distance of heating arrays, modulation frequency and other parameters.

On these bases, Kuo et al. (2011) proposed that inducing the disturbance of ponderomotive force in F region by BW can be an electrojet-independent modulation technique, VLF waves were successfully modulated when the magnetic disturbances shown on the magnetometer were weak. According to numerical simulation and experimental verification, Kuo et al. (2011) therefore concluded that BW is independent of the electrojet, they also pointed out that BW is more suitable for modulating VLF waves with higher frequency, and X-mode wave modulation is more effective than O-mode wave modulation. However, Jin et al. (2011) demonstrated that the weak intensity of the electrojet measured by the magnetometer sometimes does not mean that low-frequency waves are not generated in the D region, because the intensity of modulated low-frequency waves is also affected by D region electron profile. Subsequently, Kuo et al. (2012) further determined that the source region of VLF waves generated by BW was located in the F layer, and pointed out that the modulation effect of underdense heating was better than that of overdense heating. Moore et al. (2012) used the time-of-arrival (TOA) analysis method proposed by Fujimaru and Moore (2011) to infer that the source region of BW was in D layer instead of F layer and the theoretical model established by Cohen et al. (2012) for D region collisional absorption confirmed this conclusion. But Cohen et al. (2012) also pointed out that the F layer BW modulation theory proposed by Kuo et al. (2011, 2012) could not be ruled out at present, and needs to be further tested and verified. Therefore, it is still controversial whether the source region of ELF/VLF waves generated by BW modulation is located in D layer (Tereshchenko et al., 2014; Li et al., 2016; Xu et al.,

2019; Ma et al., 2019) or F layer (Kuo et al., 2013; Rooker et al., 2013; Yang et al., 2018, 2019b).

### 1.4.3 Thermal Cubic Non-linearity

Thermal cubic non-linearity was first proposed by Ginzburg (1964) (cited in Moore et al., 2013). This mechanism was used for generating ELF/VLF waves by Kotik and Ermakova (1991) (cited in Kotik and Ermakova, 1998) for the first time. In this method, two HF waves with frequencies $f_1$ and $f_2$ respectively where $f_2 = 2f_1 \pm f$ ($f$ is the frequency needs to be modulated) are injected into the ionosphere (Barr, 1996; Kotik and Ermakova, 1998). Moore et al. (2013) applied TOA analysis to experimental observations to determine that the source of the thermal cubic ELF and VLF is located in the collisional D region.

In contrast to the previous conclusion (Gurevich, 1978 cited in Barr, 1996; Kotik and Ermakova, 1998) which suggests that the $f_1$ wave induces a collision frequency oscillation at $2f_1$ and then the oscillation mixes with the polarization current density of the $f_2$ wave to produce an ELF/VLF source current density at frequency $|f_2 - 2f_1|$. Moore et al. (2013) proposed that the ELF and VLF source is mainly induced by the interaction between collision frequency oscillations at frequency $f_2 - f_1$ and the polarization current density associated with HF wave at frequency $f_1$.

In addition, ELF/VLF waves generated by thermal cubic non-linearity are significantly weaker than AM in the 1-5 kHz range (Cohen and Gołkowski, 2013) and 16-20 kHz range (Moore et al., 2012). ELF/VLF waves generated by thermal cubic non-linearity are also weaker than the ionospheric current drive mechanism which will

be introduced in section 1.4.4, especially at lower frequencies (< 100Hz) (Papadopoulos et al., 2011a), but cubic generation is stronger at higher frequencies (> 10 kHz) (Moore et al., 2013). Moreover, Thermal cubic non-linearity may be used to generate ELF waves using VLF waves (Barr, 1997) because VLF waves are more effective than HF waves when heating the ionosphere.

### 1.4.4 Ionospheric Current Drive

Ionospheric current drive (ICD) was proposed by Papadopoulos et al. (2011a) and verified by experiments for the first time (Papadopoulos et al., 2011b) as a method to generate low ELF/ULF frequency waves without relying on the presence of electrojets, so this mechanism can be used to modulate ELF/ULF waves in the mid-latitude region. The effect relies on modulated F region HF heating to form local diamagnetic current which then generates Magneto-Sonic (MS) waves that modulate Hall currents when they reach the D-E region. The modulated Hall currents inject ELF waves downward into the Earth-Ionosphere waveguide as well as Shear Alfven (SA) waves upward into the magnetosphere (as shown in Figure 1.8). Based on the cold plasma model, Eliasson et al. (2012) constructed the numerical model of ELF/ULF waves excited by the ICD method, as well as the propagation model of MS waves and ELF/ULF waves. By considering the characteristics of magnetic field and radio wave propagation in the mid-latitude ionosphere, Sharma et al. (2016) studied the ICD method exciting ELF waves in the mid-latitude region and its propagation in the ionosphere and magnetosphere. Xu et al. (2016) studied the generation and propagation of ULF waves modulated by the ICD mechanism under different background ionospheric parameters and modulation frequencies through numerical simulation. Streltsov et al. (2014) found that the intensity of ELF waves enhanced significantly when modulated with the frequency of Schumann resonance. They suggested that the ELF waves generated in their experiments may be the result of conductivity modulation in the lower ionosphere and ICD in the F region, but the respective contribution of the two mechanisms cannot be quantitatively analyzed due to the lack of high-resolution

ionosonde data. Moreover, the experiments of Papadopoulos et al. (2011b) adopted O wave heating, while subsequent experiments in HAARP (Streltsov et al., 2014) and EISCAT (Blagoveshchenskaya et al., 2011, 2013) have proved that X wave can also cause significant disturbance of electron temperature and electron density in the F layer, so X wave heating can also effectively trigger the ICD mechanism.

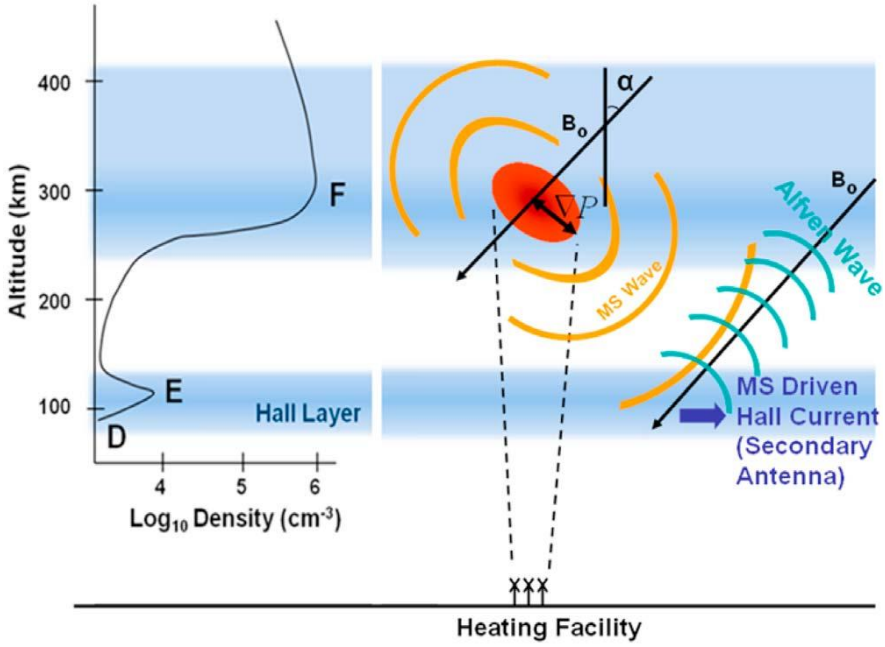


Figure 1.8 Schematic of the Ionospheric Current Drive (ICD) mechanism. Periodic heating of F region leads to an oscillatory diamagnetic current and an associated field aligned magnetic moment M that radiates isotropic MS waves. Then the MS wave drives Hall current in the E region and couples them to the SA mode. The process injects ELF waves and SA waves in the earth-ionosphere waveguide and the magnetosphere respectively (from Papadopoulos et al., 2011a).

### 1.4.5 LH-to-whistler Mode Conversion

Lower hybrid (LH) waves are parametrically excited by HF-pump-plasma interactions at the upper hybrid (UH) layer. Vartanyan et al. (2016) analyzed two heating experiments at HAARP with the observation from DEMETER and found that F region ionospheric heating by continuous waves could also generate VLF waves of certain frequencies, the whole process is independent of the electrojet. This method is based

on the mode conversion of LH waves, so it can only be used for generating VLF waves in the corresponding frequency range of LH and its harmonic as shown in Figure 1.9 (7-10 kHz and 15-19 kHz respectively). The mechanism of this method is described as follows, the HF continuous-wave interacts with the plasma in the upper hybrid layer to excite LH waves, then the VLF wave is generated by mode conversion of LH waves. Vartanyan et al. (2016) proposed two points: 1) the VLF waves observed at the LH frequency are due to the interaction of the LH waves with meter-scale field-aligned striations, 2) the VLF waves at twice the LH frequency are due to the interaction of two counter propagating LH waves. This mechanism was also verified by Kuo and Lee (2017) by experiments.

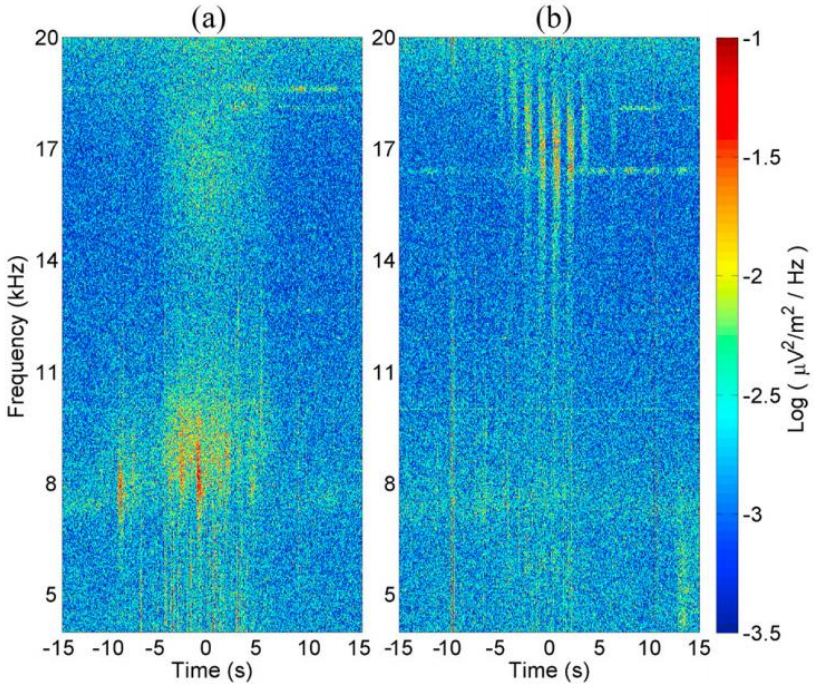


Figure 1.9 Spectrogram obtained by DEMETER during (a) Experiment 1 with CW heating and (b) Experiment 2 with 0.7 Hz square pulse modulated heating. In both cases time = 0 corresponds to the closest approach of DEMETER to the magnetic zenith of HAARP (from Vartanyan et al., 2016).

Furthermore, Gigliotti et al. (2009) carried out an experiment using the Large Plasma Device (LAPD) at University of California, Los Angeles (UCLA) to generate polarized shear Alfven waves (SAW) using a rotating magnetic field (RMF) source

created via a phased orthogonal two-loop antenna. This was the first time to form RMF controlled by a special antenna. Although this was not a method for generating ELF/VLF waves by modulating HF waves, it was another way to generate ELF/VLF waves instead of transmitted by ELF/VLF antenna directly. Gigliotti et al. (2009) also pointed out the prospect of using satellites to carry such antennas to form RMF in the space and inject SAW into radiation belts. Subsequent three-dimensional numerical simulations and relevant experiments have demonstrated that the RMF mechanism can effectively generate SAW and low-frequency whistler waves (Karavaev et al., 2010, 2011). In recent years, the LAPD has further upgraded its devices (Martin et al., 2015; Gekelman et al., 2016) for further research in the future. Inspired by this method, De Soria-Santacruz, et al. (2014) theoretically designed a spaceborne antenna to excite low-frequency waves.

## 1.5 The Controversy about Beat Wave Modulation

As described in Section 1.4.2, it is still controversial to determine the mechanism of BW and its source region for generating ELF/VLF waves.

By comparing the excitation efficiency of ELF/VLF waves by AM and BW in each frequency band using HIPAS heating facility, the experimental results showed that the ELF/VLF signal excited by AM is strongest at almost all frequencies, although BW can produce more stable signals under certain circumstances (Villaseñor et al., 1996). Barr and Stubbe (1997) confirmed this conclusion by experiments at EISCAT.

Kuo et al. (2011) proposed that the mechanism of BW is ponderomotive nonlinearity in the F region, which means BW is an electrojet-independent modulation method. Based on this theory, Kuo et al. (2012) conducted experiments and found that BW is more effective than AM in the VLF range. Cohen et al. (2012) also pointed out that BW produces stronger amplitudes than AM when the modulated frequency is higher

than 5 kHz.

On the other hand, according to the theory of BW by electrojet modulation in the D region, the modulation efficiency decreases with the increase of the modulated frequency, while according to the theory of BW by ponderomotive force in the F region, the modulation efficiency increases with the increase of the modulated frequency.

However, according to the experimental results obtained by Ma et al. (2019) using EISCAT equipment, the BW modulation efficiency may vary greatly in a short time, and the variation trend with the modulated frequency is not obvious (Figure 1.10).

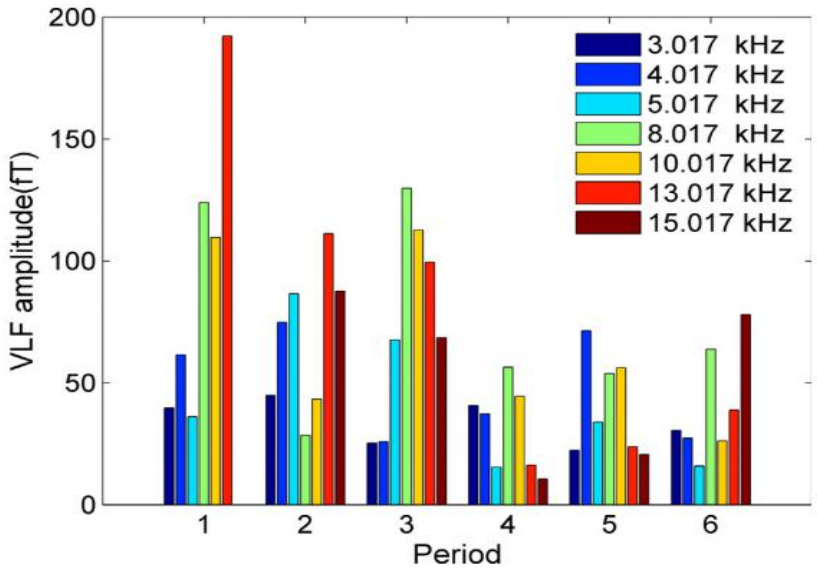


Figure 1.10 Variations in very low frequency (VLF) amplitude excited by varying beat wave (BW) frequencies during the six periods with $f_0 = 4.04$ MHz (from Ma et al., 2019)

In summary, the mechanism of BW cannot be inferred from the existing experimental observations reported in the literature. This dissertation is to explore the ELF/VLF generation by BW modulation. In this context, simulation of ionospheric heating and its physical model is constructed so that AM and BW by electrojet modulation in the

D region as well as BW by ponderomotive force in the F region can be simulated respectively; finally, a new method to identify the mechanism and source region of BW is proposed.

# Chapter 2

# Numerical Model of Ionospheric Heating

The increase of electron temperature during ionospheric heating is mainly due to the Ohmic heating effect. It is essentially the collision and absorption of high frequency waves by particles in the ionosphere. When HF waves are transmitted into the ionosphere, the electron will absorb wave energy so that its temperature and kinetic energy will increase, as a result, the collision frequency with other particles also increases. In the process of collision with other particles, part of the energy will be transferred from the electron to other particles, finally, the plasma parameters of the ionosphere will change. The changes of electron temperature and density are the main effects of Ohmic heating. This process can be expressed by three basic equations (energy equation, dynamic equation, continuity equation). However, because of the differences in plasma parameters and physical processes at different heights, the basic equations in the lower and upper ionosphere are slightly different. So, in this chapter, the construction of the ionospheric heating model based on Ohmic heating in lower and upper ionosphere is described. It is worth noting that firstly, the lower ionospheric heating model is for underdense heating and the upper ionospheric heating model is for overdense heating, so all the simulations in this thesis based on lower ionospheric heating are underdense heating, correspondingly, all the simulations in this thesis based on upper ionospheric heating are overdense heating. Secondly, wave-resonances, such as the Upper-Hybrid resonance, are not discussed in this thesis.

All the numerical simulations and figures in this dissertation were obtained by carrying out MATLAB software, which ran on a PC with an I7 6700HQ 4-core CPU.

# 2.1 D and E-region Ionospheric Heating

In the lower ionosphere, the effect of collisions is important, while the transport process can be ignored. When the electromagnetic waves pass through, the lost energy is mainly absorbed by the electrons, and the electron loses energy through the collision with ions and neutral particles, and reaches the energy balance after a certain time so that the temperature rises to a constant value. Accordingly, since the electron recombination coefficient is a function of the electron temperature, the electron number density will change during heating.

## 2.1.1 Basic Equation

### 2.1.1.1 Electronic Energy Equation

The electronic energy equation in the lower ionosphere can be written as (Pashin et al., 1995):

$$\frac{3}{2}k_b n_e \frac{\partial T_e}{\partial t} = Q(T_e, l) - L(T_e, l) \tag{2.1}$$

$k_b$ is Boltzmann constant, $n_e$ and $T_e$ are electron density and electron temperature respectively, $l$ is the height, $Q(T_e, l)$ and $L(T_e, l)$ are absorption term and loss term of electronic energy respectively. $Q(T_e, l)$ includes both the energy of sunlight and HF waves. The energy of sunlight can be calculated by setting the left-hand side of the equation as 0, i.e. steady state.

### 2.1.1.2 Continuity Equation

The electron density in the lower ionosphere is determined from the continuity equation (Pashin et al., 1995):

$$\frac{\partial n_e}{\partial t} = q - \alpha(T_e) n_e^{\,2} \tag{2.2}$$

where $q$ is production rate, $\alpha(T_e)$ is recombination coefficient. The production rate of sunlight can be calculated by setting the left-hand side of the equation as 0, i.e. steady state. In lower ionosphere, the molecular ions ($NO^+$ and $O_2^+$) are the most important in recombination process, so $\alpha(T_e)$ can be expressed as (Gurevich, 1978 cited in Pashin et al., 1995):

$$\alpha(T_e) = 5\times10^{-7}[\mathrm{NO}^+](300/T_e)^{1.2} + 2.2\times10^{-7}[\mathrm{O_2}^+](300/T_e)^{0.7} \tag{2.3}$$

where $[\mathrm{X}]$ represents the density of particle X.

## 2.1.2 Calculation of Energy

### 2.1.2.1 Absorption Term

The absorbed energy of unit volume during unit time in height $l$ is (Huang and Gu, 2003a):

$$Q(l) = 2\kappa S(l) \tag{2.4}$$

the energy of radio waves in height $l$ is (Huang and Gu, 2003a):

$$S(l) = \frac{ERP}{4\pi l^2}\exp[-2\int_{l_0}^{l}\kappa(l')dl'] \tag{2.5}$$

$ERP$ is the Effective Radiated Power; $\kappa(l)$ is wave absorption index and can be expressed as (Huang and Gu, 2003a):

$$\kappa = \frac{\omega}{c}\chi \tag{2.6}$$

$\omega = 2\pi f$, $f$ is the frequency of HF radio wave, $c$ is the velocity of light, $\chi$ is the imaginary part of the complex refraction index according to Appleton-Hartree (A-H) equation (Ye and Liu, 1983):

$$\begin{aligned} n^2 &= (\gamma + i\chi)^2 \\ &= 1 - 2X\frac{1 - iZ - X}{2(1-iZ)(1-iZ-X) - {Y_T}^2 \pm \sqrt{{Y_T}^4 + 4{Y_L}^2(1-iZ-X)^2}} \end{aligned} \tag{2.7}$$

where $X = {f_N}^2/f^2, Y = f_H/f, Z = \upsilon_e/2\pi f$, $Y_T = Y\sin\varphi, Y_L = Y\cos\varphi$, $\varphi$ is the

angle of normal direction of the incident wave and the earth's magnetic field, $f$ is the frequency of radio wave, $f_N = (n_e \cdot e^2 / 4\pi^2 \varepsilon_0 m)^{1/2}$ is the frequency of plasma, $f_H = eB/m$ is the cyclotron frequency of electrons. As for symbol "±", "+"means the incident wave is ordinary wave (O wave), "_" means the incident wave is extraordinary wave (X wave). The collision frequency of electron $\upsilon_e$ in A-H equation can be calculated by empirical equation (Pashin et al., 1995):

$$\upsilon_e = 1.7\times10^{-11}[\mathrm{N_2}]T_e + 3.8\times10^{-10}[\mathrm{O_2}]T_e^{1/2} + 1.4\times10^{-10}[\mathrm{O}]T_e^{1/2} \tag{2.8}$$

The calculation of geomagnetic field adopts the central dipole field model (Liu et al., 1997):

$$B = B_0\left(\frac{R_e}{R_e + h}\right)^3 \sqrt{1 + 3\sin^2\lambda} \tag{2.9}$$

where $B_0 = 3.085\times10^{-5}T$, $R_e$ is mean radius of the earth, $\lambda$ is magnetic latitude, $h$ is height.

**2.1.2.2 Loss Term**

The loss of electron energy in the ionosphere is mainly realized by collisions, its mechanism is very complex, mainly including (Stubbe and Varnum, 1972):

（1） Elastic collision of electrons with positive ions

$$L_1 = -n_e n_i \times (7.7 \pm 0.8)\times10^{-6} T_e^{-3/2} M_i^{-1}(T_e - T_i) \tag{2.10}$$

where $n_i, M_i, T_i$ are the density, mass and temperature of ions respectively.

（2） Elastic collision of electrons with neutral particles

Neutral particles in the ionosphere below F region are mainly molecular oxygen and nitrogen ($O_2$ and $N_2$), as well as atomic oxygen O, the collision losses of electrons with these three particles are respectively:

$$L_2 = -n_e[\mathrm{O_2}]\times1.2\times10^{-18} T_e^{1/2}(T_e - T_n)(1 + 3.6\times10^{-2} T_e^{1/2}) \tag{2.11}$$

$$L_3 = -n_e[\mathrm{N_2}]\times1.8\times10^{-19} T_e(T_e - T_n)(1 - 1.21\times10^{-4} T_e) \tag{2.12}$$

$$L_4 = -n_e[\mathrm{O}]\times 5.3\times 10^{-19} T_e^{1/2}(T_e - T_n)(1+5.7\times 10^{-4} T_e) \tag{2.13}$$

where $T_n$ is the temperature of neutral particles.

（3） The excitation of the rotational level of $O_2$ and $N_2$

$$L_5 = -n_e[\mathrm{O}_2]\times 7\times 10^{-14} T_e^{-1/2}(T_e - T_n) \tag{2.14}$$

$$L_6 = -n_e[\mathrm{N}_2]\times 2.8\times 10^{-14} T_e^{-1/2}(T_e - T_n) \tag{2.15}$$

（4） The excitation of the vibration level of $O_2$ and $N_2$

$$L_7 = n_e[\mathrm{O}_2]\times 7.45\times 10^{-13}\exp(f_1\frac{T_e-700}{700T_e})[\exp(-3000\frac{T_e-T_n}{T_eT_n})-1] \tag{2.16}$$

$f_1 = 3.902\times 10^3 + 4.38\times 10^2 \tanh[4.56\times 10^{-4}(T_e - 2400)]$,

$$L_8 = n_e[\mathrm{N}_2]\times 2.99\times 10^{-12}\exp(f_2\frac{T_e-2000}{2000T_e})[\exp(-g\frac{T_e-T_n}{T_eT_n})-1] \tag{2.17}$$

$f_2 = 1.06\times 10^4 + 7.51\times 10^3 \tanh[1.1\times 10^{-3}(T_e - 1800)]$,

$g = 3300 + 1.233(T_e - 1000) - 2.056\times 10^{-4}(T_e - 1000)(T_e - 4000)$.

（5）The excitation of electronic energy level and fine structure of atom O

$$L_9 = n_e[\mathrm{O}]\times 1.57\times 10^{-12}\exp(f_3\frac{T_e-3000}{3000T_e})[\exp(-22713\frac{T_e-T_n}{T_eT_n})-1] \tag{2.18}$$

$f_3 = 2.4\times 10^4 + 0.3(T_e - 1500) - 1.947\times 10^{-5}(T_e - 1500)(T_e - 4000)$,

$$L_{10} = -n_e[\mathrm{O}]\times 3.4\times 10^{-12} T_n^{-1}(T_e - T_n)(1-7\times 10^{-5} T_e) \tag{2.19}$$

The loss of electron energy is the sum of the above loss mechanisms:

$$L_g = L_1 + L_2 + \ldots + L_{10} \tag{2.20}$$

Its unit is $\mathrm{eVcm^{-3}s^{-1}}$, it should be noted that this is the Gauss System of Units, which should be multiplied by the corresponding coefficient if needs to be transferred to International System of Units

$$L = L_g \times 1.6\times 10^{-13} \tag{2.21}$$

Now its unit is $\mathrm{Jm^{-3}s^{-1}}$. The loss of electron energy in the D region is dominated by

the excitation of the vibration level of $O_2$ ($L_7$), while in the E region it is dominated by the excitation of the rotational level of $O_2$ and $N_2$ ($L_5$ and $L_6$). The loss of electron energy in the F region is much greater than in the D and E region, which is dominated mainly by the excitation of fine structure of atom O ($L_{10}$).

## 2.2 F- region Ionospheric Heating

The change of electron temperature and density at ionospheric F-region heating are mainly controlled by three equations along the direction of the magnetic field: momentum equation, electron energy equation and continuity equation.

### 2.2.1 Basic Equation

#### 2.2.1.1 momentum equation

The momentum equation in the upper ionosphere can be written as (Wang et al., 2012):

$$n_e v_e = \alpha\{\frac{\partial}{\partial s}[n_e k_b (T_e + T_i)] + \sum_a n_a m_a \mathrm{g}\} + n_e v_n \cos I \tag{2.22}$$

$s$ is along the magnetic field, $v_e$ is electron velocity in the direction of the magnetic field, $k_b$ is Boltzmann constant, $n_a, m_a$ are density and mass of charged particle, g is the gravitational acceleration, $v_n$ is velocity of neutral wind, $I$ is magnetic dip, $\alpha = -1/(m_e \upsilon_{en} + M_I \upsilon_{In})$ is diffusion coefficient, $M_I \upsilon_{In}$ is the collision weighting factor of ions and neutral particles, according to quasi neutral condition (Huang and Gu, 2003b):

$$\frac{1}{M_I \upsilon_{In}} = \sum_i \frac{(n_i / n_e)}{m_i \upsilon_{In}} \tag{2.23}$$

#### 2.2.1.2 Energy Equation

The electron temperature can be calculated by energy equation (Bernhardt and Duncan, 1982):

$$\frac{3}{2}k_b[n_e\frac{\partial T_e}{\partial t}+n_e v_e\frac{\partial T_e}{\partial s}]+k_b n_e T_e\frac{\partial v_e}{\partial s}=\frac{\partial}{\partial s}(K_e\frac{\partial T_e}{\partial s})+S_{HF}+S_0+L \quad (2.24)$$

The first term on the left side of the above equation is the time-dependent term for electron temperature due to heating, the second term on the left side is the convective term, the third term on the left side is the pressure term; the first term on the right side is the heat transfer term, $S_{HF}$ means energy absorbed per unit time, $S_0$ means energy absorption without heating, $L$ means loss of energy, $K_e$ is the thermal conductivity in the direction of the magnetic field (Banks and Kockarts, 1973 cited in Wang et al., 2012):

$$K_e=\frac{7.7\times10^5 T_e^{5/2}}{1+3.22\times10^4(T_e^2/n_e)\sum_i n_{ni}\overline{Q_D}}\ \text{eV/cm/s/K} \quad (2.25)$$

$n_{ni}$ represents the density of neutral particle $i$, $\overline{Q_D}$ is the average momentum transfer cross section of neutral particle (Djuth et al., 1990):

$$Q_{O_2}=2.2\times10^{-16}(1+3.6\times10^{-2}\sqrt{T_e}) \quad (2.26)$$

$$Q_{N_2}=10^{-17}(2.82-3.41\times10^{-4}T_e)\sqrt{T_e} \quad (2.27)$$

$$Q_O=10^{-15} \quad (2.28)$$

Their units are $\text{cm}^2$.

#### 2.2.1.3 Continuity Equation

The continuity equation in the upper ionosphere can be written as (Huang and Gu, 2003b):

$$\frac{\partial n_e}{\partial t}=Q_0-(k_1 n_{NO^+}+k_2 n_{O_2^+})n_e-\frac{\partial(n_e v_e)}{\partial s} \quad (2.29)$$

$Q_0$ is production rate of electron during equilibrium state ($\frac{\partial n_e}{\partial t}=0$), the second term

on the right of the equation is the rate of electron loss caused by the recombination process, the third term on the right of the equation is the decrease of electron density per unit time caused by transport process. There are three main ions ($NO^+$, $O_2^+$, $O^+$) in the ionosphere at F-region altitude, $O^+$ gradually dominant with an increase in altitude, its recombination process includes two steps:

【1】Ion-atom exchange

$$O^+ + N_2 \rightarrow NO^+ + N \tag{2.30}$$

$$O^+ + O_2 \rightarrow O_2^+ + O \tag{2.31}$$

【2】Decomposition-recombination

$$NO^+ + e^- \rightarrow N + O \tag{2.32}$$

$$O_2 + e^- \rightarrow O + O \tag{2.33}$$

The reaction rate of ion-atom exchange is independent of the electron temperature. Therefore, the change of electron density caused by heating is mainly dependent on the transport process (Huang and Gu, 2003b), the recombination term (the second term on the right of the equation) only considers the decomposition-recombination, $k_1, k_2$ are recombination coefficients of $NO^+$ and $O_2^+$ respectively (Huang and Gu, 2003b):

$$k_1 = 4.2 \times 10^{-7} (300/T_e)^{0.85} \text{ cm}^3/\text{s} \tag{2.34}$$

$$k_2 = 1.6 \times 10^{-7} (300/T_e)^{0.55} \text{ cm}^3/\text{s} \tag{2.35}$$

## 2.2.2 Calculation of wave energy

### 2.2.2.1 Absorption term

After the high-frequency wave is injected into the ionosphere, the electrons in the ionosphere absorb the wave energy, which causes the increase of electron temperature and the disturbance of electron density. In order to obtain the spatial distribution of the electron absorption energy in the ionosphere, the path of the wave propagation in the ionosphere needs to be determined through the ray tracing program.

Ray tracing is an important method to study wave propagation in the ionosphere. A set of numerical programs proposed by Jones and Stephenson. (1975) for solving ray trajectories based on the ionospheric model, collision model and geomagnetic field model are widely used, it consists of the following six equations with the path of the wave propagation group $P'$ as the independent variable (Jones and Stephenson, 1975):

$$\frac{dr}{dP'} = -\frac{1}{c}\frac{\partial H/\partial k_r}{\partial H/\partial \omega} \tag{2.36}$$

$$\frac{d\theta}{dP'} = -\frac{1}{rc}\frac{\partial H/\partial k_\theta}{\partial H/\partial \omega} \tag{2.37}$$

$$\frac{d\varphi}{dP'} = -\frac{1}{rc\sin\theta}\frac{\partial H/\partial k_\varphi}{\partial H/\partial \omega} \tag{2.38}$$

$$\frac{dk_r}{dP'} = \frac{1}{c}\frac{\partial H/\partial k_r}{\partial H/\partial \omega} + k_\theta\frac{d\theta}{dP'} + k_\varphi\frac{d\varphi}{dP'} \tag{2.39}$$

$$\frac{dk_\theta}{dP'} = \frac{1}{r}(\frac{1}{c}\frac{\partial H/\partial k_r}{\partial H/\partial \omega} - k_\theta\frac{dr}{dP'} + k_\varphi r\cos\theta\frac{d\varphi}{dP'}) \tag{2.40}$$

$$\frac{dk_\varphi}{dP'} = \frac{1}{r\sin\theta}(\frac{1}{c}\frac{\partial H/\partial k_\varphi}{\partial H/\partial \omega} - k_\varphi\sin\theta\frac{dr}{dP'} + k_\theta r\cos\theta\frac{d\theta}{dP'}) \tag{2.41}$$

$r,\theta,\varphi$ are the three components in a spherical coordinate system respectively.

$k_r,k_\theta,k_\varphi$ are the components of the path of the wave propagation group $P'$ in three directions in spherical coordinates respectively. $c$ represents the velocity of light, $\omega$ is angular frequency of waves, $H$ is Hamilton operator (Jones and Stephenson, 1975):

$$H = \frac{1}{2}[\frac{c^2}{\omega^2}(k_r{}^2 + k_\theta{}^2 + k_\varphi{}^2) - real(n^2)] \tag{2.42}$$

Complex refraction index $n$ can be calculated by the A-H equation (see equation 2.7).

When the wave frequency is high, the influence of the magnetic field can be ignored when calculating the wave path, while the collision effect only causes energy loss, so it also can be ignored when calculating the wave path. Therefore, the phase refractive index can be simplified as:

$$n^2 = 1 - X \tag{2.43}$$

*H* can be simplified as:

$$H = \frac{1}{2}\left(\frac{c^2}{\omega^2}k^2 - n^2\right) \tag{2.44}$$

so the equations of ray tracing can be expressed as:

$$\frac{dr}{dP'} = \frac{c}{\omega}k_r \tag{2.45}$$

$$\frac{d\theta}{dP'} = \frac{c}{\omega r}k_\theta \tag{2.46}$$

$$\frac{d\varphi}{dP'} = \frac{c}{\omega r \sin\theta}k_\varphi \tag{2.47}$$

$$\frac{dk_r}{dP'} = -\frac{\omega}{2c}\frac{\partial X}{\partial r} + (k_\theta{}^2 + k_\varphi{}^2)\frac{c}{\omega r} \tag{2.48}$$

$$\frac{dk_\theta}{dP'} = \frac{1}{r}\left(-\frac{\omega}{2c}\frac{\partial X}{\partial \theta} - k_r k_\theta \frac{c}{\omega} + k_\varphi{}^2 \cot\theta \frac{c}{\omega}\right) \tag{2.49}$$

$$\frac{dk_\varphi}{dP'} = \frac{1}{r\sin\theta}\left(-\frac{\omega}{2c}\frac{\partial X}{\partial \varphi} - k_r k_\theta \sin\theta \frac{c}{\omega} - k_\theta k_\varphi \cos\theta \frac{c}{\omega}\right) \tag{2.50}$$

Let us set the wave elevation as $\beta$, set the transmitter azimuth as $\alpha$, set the frequency of wave as $\omega$, the longitude and latitude are $\lambda_0$ and $\varphi_0$ respectively, the radius of the earth is $r_0$. The initial values for calculating the ray trajectory can be obtained as:

$$r = r_0 \tag{2.51}$$

$$\theta = \frac{\pi}{2} - \lambda_0 \tag{2.52}$$

$$\varphi = \varphi_0 \tag{2.53}$$

$$k_r = |\mathbf{k}|\cos\left(\frac{\pi}{2} - \beta\right) \tag{2.54}$$

$$k_\theta = -|\mathbf{k}|\cos\beta\cos\alpha \tag{2.55}$$

$$k_{\varphi} = -|\mathbf{k}| \cos\beta \sin\alpha \tag{2.56}$$

The reflection surface of the incident wave beam in the ionosphere can be obtained through the above ray tracing program, the absorption is strongest at the reflection point in the beam center (Bernhardt and Duncan, 1982):

$$S_{\max} = (\upsilon_e \varepsilon_0 / 2)(f_N{}^2 / f^2) E(z_m)^2 \tag{2.57}$$

$\upsilon_e$ means electron collision frequency, $\varepsilon_0$ is the permittivity in free space, $f_N$ is plasma frequency, $f$ is frequency of wave, $E(z_m)$ is the intensity of electric field at the reflection point in the beam center, it can be calculated by empirical equation (Belenov, 1997):

$$E(z) = \sqrt{30 ERP} / z \tag{2.58}$$

$ERP$ is effective radiated power of radio wave, $z$ is the height.

The energy absorption in any location in the ionosphere can be calculated by Gaussian distribution (Djuth et al., 1990; DuBois et al., 1990):

$$S_{HF}(x,z) = A \cdot S_{\max} \exp[-(z-z_m)^2 / \sigma_z{}^2] \exp[-(x-x_0)^2 / \sigma_x{}^2], z \le z_m \tag{2.59}$$

$$S_{HF}(x,z) = 0, z > z_m \tag{2.60}$$

$(x,z)$ represents any point in the ionosphere, $A$ is the proportional constant, $(x_0, z_m)$ is the position of the reflection point, $\sigma_x$ and $\sigma_z$ are the horizontal half-width and vertical half-width respectively.

#### 2.2.2.2 Loss term

The expressions of loss mechanisms are shown in section 2.1.2.2.

## 2.3 Numerical Simulation

In this section, the change of electron temperature during ionospheric heating in the lower and upper ionosphere is simulated respectively, in addition, in order to verify

the reliability of the numerical model, the simulation results were compared with some references.

### 2.3.1 D/E region ionospheric heating

The mechanism and physics process of lower altitude ionospheric heating has been researched for decades. In this part, our simulation results were compared with Huang et al. (2004).

The ERP (Effective Radiated Power), frequency and mode of HF waves are: 200 MW, 4.0 MHz, and X wave, respectively. The background ionosphere is in the sunlight of a magnetically quiet day in the mid-latitude region. The parameter of the ionosphere and atmosphere are taken from IRI-2016 model and NRLMSISE-00 model respectively. Heating time is 1 s with a time step of $1\,\mu s$ , the height range is 65~120 km with a spatial resolution of 1 km. During the heating process, the electron temperature reaches the steady state in milliseconds, but the electron density does not reach the steady state. The $f_oE$ is 3.4 MHz, which means this is an underdense heating process.

Figure 2.1 and 2.2 are the results of Huang et al. (2004) and our simulation results, respectively. From these two figures, it is found that the electron temperature increases significantly in the D region and slightly in the E region after HF heating, which means the main absorption region of HF waves is the D region and the peak is located at the altitude of 70-80 km. This characteristic reflects the “D region absorption effect” according to Tomko et al. (1980) which can be a very useful effect for us to determine the location of the source of beat wave modulation in Chapter 4. In addition, the results show that our physical model of lower ionospheric heating is effective.

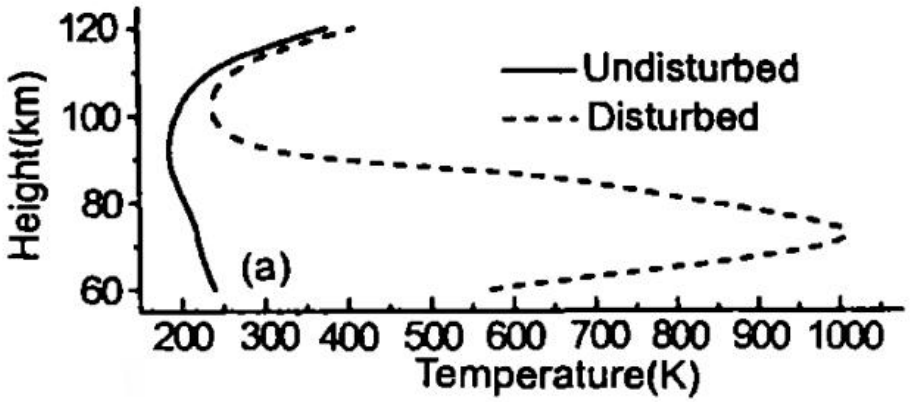


Figure 2.1 Electron temperature in D and E regions before (full line) and after (dotted line) lower ionospheric heating for 1 s (from Huang et al. 2004).

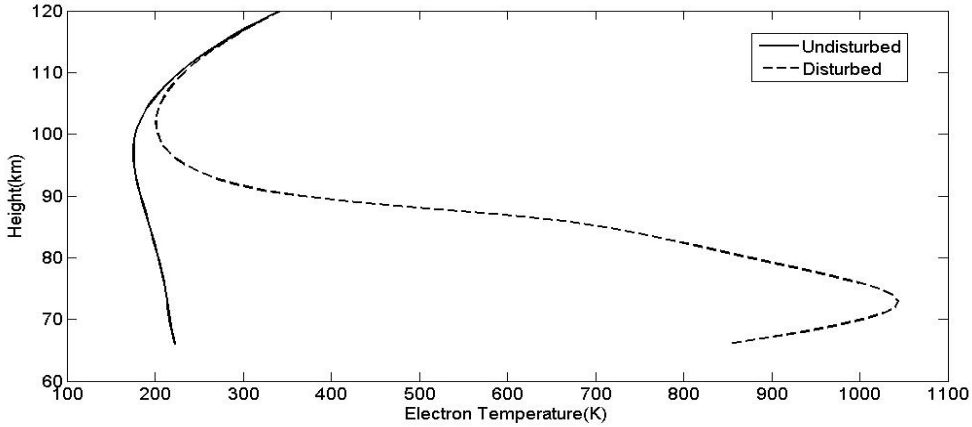


Figure 2.2 Simulation of electron temperature in D and E regions before (full line) and after (dotted line) lower ionospheric heating for 1 s with the same parameters as Huang et al. (2004).

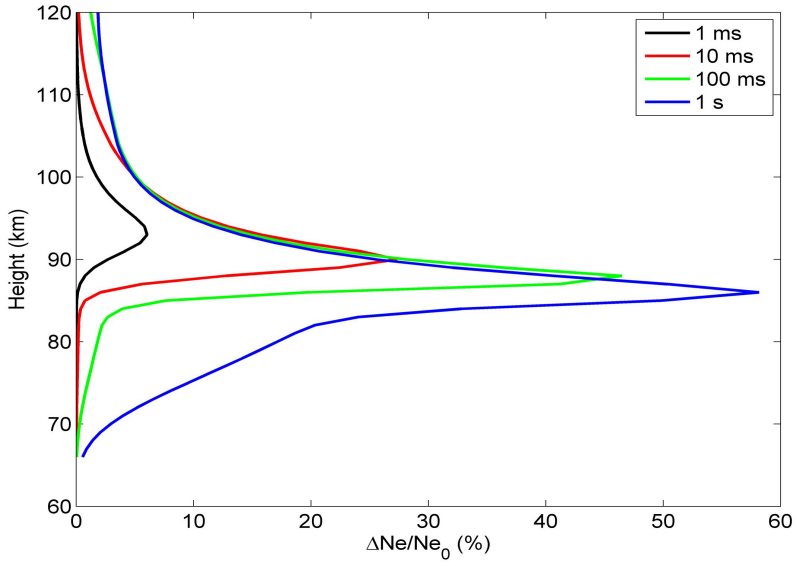


Figure 2.3 Simulation of relative disturbances of electron density in D and E regions after lower ionospheric heating for different heating periods of 1 ms to 1 s with the same parameters as Huang et al. (2004).

Figure 2.3 shows the relative disturbance of electron density in the lower altitude during ionospheric heating. As can be seen, during the heating process, the electron density increases at all heights over time, the height of the peak of enhanced electron density decreases with increasing time. In this dissertation, mainly modulations of ELF/VLF waves greater than 1000 Hz are discussed, so the relative disturbance of electron density during modulated heating is usually less than 5%, which means it is negligible when the disturbance of conductivity and current is calculated. On the other hand, it is significant if we take ELF/ULF waves less than 1000 Hz into consideration.

### 2.3.2 F region ionospheric heating

Our simulation results (Figure 2.5) were compared with the experimental results of Wang et al. (2012) (Figure 2.4) to verify the validity of the model of higher altitude ionospheric heating. The chosen time is 10:36 UT on January 10, 2008, the location is 69.6°N, 19.2°E (EISCAT heating facility). The parameters of the ionosphere and atmosphere are derived from IRI-2016 and NRLMSISE-00 model. The parameters of

the HF heating wave are 4.04 MHz, 170 MW, O wave. Heating time is 4 min with a time step of 0.01 s, the height range is 120~400 km with a spatial resolution of 10 km ×10 km. During the heating process, the electron temperature reaches the steady state in tens of seconds, but the electron density does not reach the steady state. The $f_oF2$ is 4.2 MHz, which means this is an overdense heating process.

The reflection point of HF wave is located at a height of about 210 km, as shown in Figure 2.4 and 2.5, it is also where the electron temperature increases the most, with an enhancement of more than 2000 K. The results show that our physical model of upper ionospheric heating is effective.

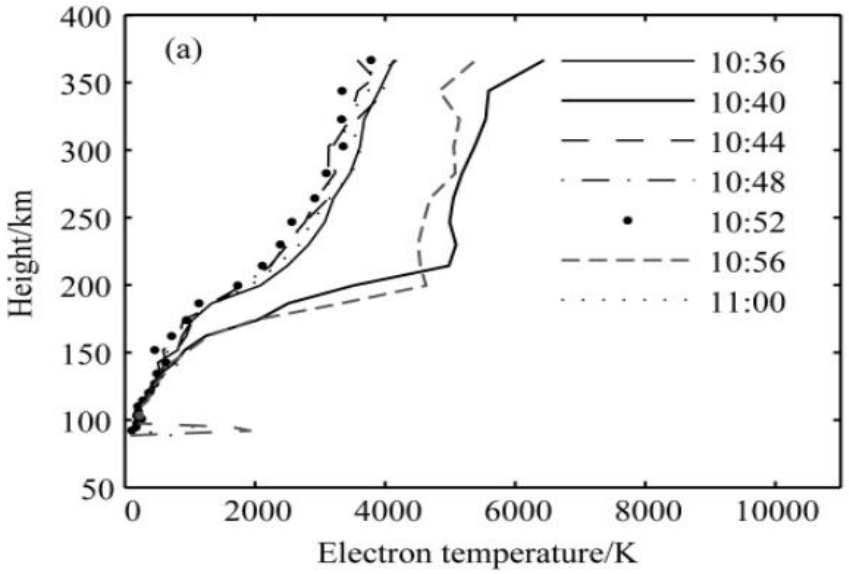


Figure 2.4 Observed electron temperature before and after ionospheric heating. Lines on 10:40 and 10:56 are for after heating, other lines are for before heating (from Wang et al., 2012).

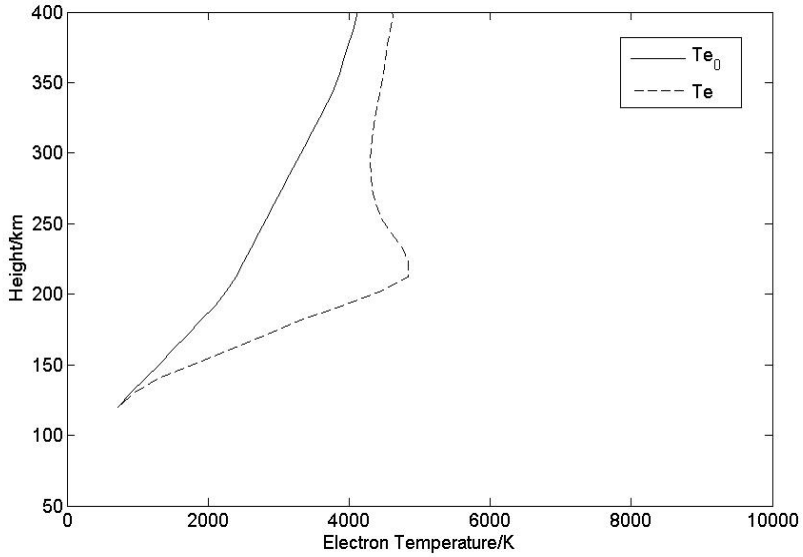


Figure 2.5 Simulation of electron temperature in F region before (full line) and after (dotted line) upper ionospheric heating with the same parameters as Wang et al. (2012).

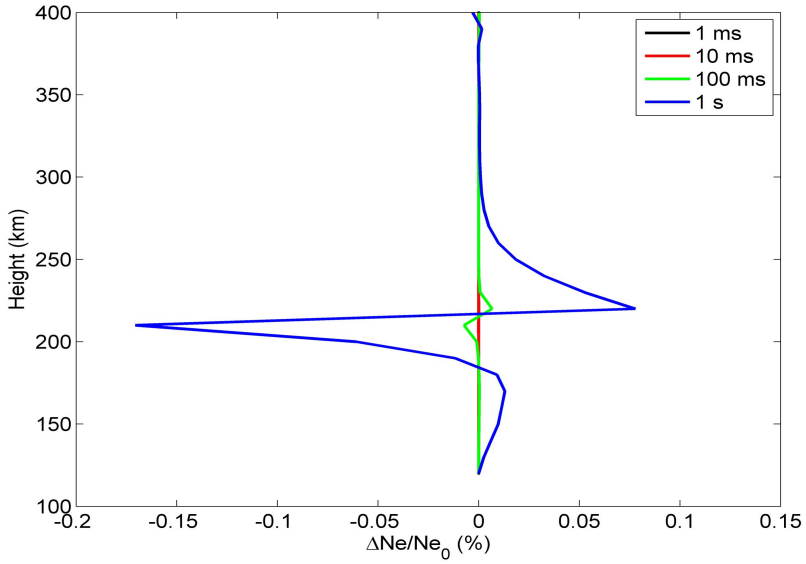


Figure 2.6 Simulation of relative disturbances of electron density in F region after upper ionospheric heating for different heating periods of 1 ms to 1 s with the same parameters as Wang et al. (2012).

Figure 2.6 shows the relative disturbance of electron density after ionospheric heating at F-region for duration of 1 ms~1 s. Unlike lower-altitude ionospheric heating, which

always causes an increase in the electron density, there is a loss zone of electron density near the reflection height corresponding to the peak of the electron temperature enhancement, while the electron density increases at both upper and lower parts of the reflection height. This is because the diffusion coefficient near the reflection point increases due to the large increase of electron temperature, causing electrons to diffuse and pushing it to the upper and lower regions along the magnetic field line.

The reason for choosing such a short heating period is to highlight the time scale of the modulated heating. As it can be seen from the figure, even at a modulation frequency of 1 Hz (assuming a duty cycle of 50% which means a heating time of only 0.5 s), the maximum rate of change of electron density is less than 0.2%. In addition, ELF/VLF waves with modulation frequency greater than 1000 Hz are mainly considered in this dissertation and it is difficult to observe the change of electron density when heating 1 ms from the figure, so the change of electron density can be ignored.

## 2.4 Summary

In this chapter, we introduced the basic mechanism and equations of modeling lower and higher-altitude ionospheric heating. Comparisons of our simulations with those published in the literature illustrates the validity of our physical models of ionospheric heating which will be used for the investigation of the effective generation mechanism of ELF/VLF waves by modulated heating. In addition, the simulation of the change of electron density during both lower and higher-altitude ionospheric heating indicates that the change of electron density is negligible for modulated heating.

# Chapter 3

# Generation of ELF/VLF waves by Amplitude Modulation and Beat Wave Modulation

Based on the physical model of ionospheric heating established in Chapter 2, we conducted simulation research on AM and BW respectively. AM is the most basic technique of ionospheric modulated heating, its substance is electrojet modulation based on thermal nonlinearity so that the source region of modulated ELF/VLF waves is located in the D region. However, the mechanism of BW is controversial; there are two different theories about the mechanism and source region of BW. One theory holds that BW is still an electrojet modulation method like AM, so the source region of generating ELF/VLF waves is located in the D region. By contrast, another theory holds that BW is an electrojet-independent modulation method, its mechanism is ponderomotive nonlinearity, and the source region of generating ELF/VLF waves is located in the F region. We introduced these two theories separately. In this Chapter, firstly, the basic equations of different modulation techniques and theories are introduced. Then, physical models are constructed and the validity is demonstrated through the comparison of numerical simulation and references, this chapter also prepares for the research in Chapter 4.

# 3.1 Amplitude Modulation

## 3.1.1 Physical Model

The essence of AM is to repeat the "heating-cooling" process in the ionosphere at a certain ELF/VLF frequency by switching on and off high power high frequency radio wave transmitters at this ELF/VLF frequency. Since the ionospheric conductivity is a function of electron temperature, it changes at the same frequency during the "heating-cooling" process, in the presence of the ionospheric electric field, the ionospheric electrojet will be modulated and generates ELF/VLF waves.

The physical model of ionospheric heating has been described in Chapter 2, therefore, this chapter only considers heating modulation. Firstly, the electric current in the ionosphere is (Ferraro et al., 1982):

$$J_0 = \sigma \cdot E_0 \tag{3.1}$$

Where $E_0$ is the natural electric field, $\sigma$ is the ionospheric conductivity. Two components of the ionospheric conductivity need to be considered in the modulation of electrojet, they are Pedersen conductivity $\sigma_{\mathrm{P}}$ and Hall conductivity $\sigma_{\mathrm{H}}$ (Li et al., 2016):

$$\sigma_P = \frac{eN_e}{B}\left(\frac{\upsilon_{en}\omega_e}{\upsilon_{en}^2+\omega_e^2}+\frac{\upsilon_{in}\omega_i}{\upsilon_{in}^2+\omega_i^2}\right) \tag{3.2}$$

$$\sigma_{\mathrm{H}} = \frac{eN_e}{B}\left(\frac{\omega_e^2}{\upsilon_{en}^2+\omega_e^2}-\frac{\omega_i^2}{\upsilon_{in}^2+\omega_i^2}\right) \tag{3.3}$$

The first term on the right hand side represents the electron conductivity, and the second term represents the ion conductivity. $\omega_e$ and $\omega_i$ are the gyrofrequency of electron and ions respectively, $\upsilon_{in}$ is the collision frequency between ions and neutral particles, the geomagnetic field $B$ can be calculated by equation (2.9). In the heating process, the electron temperature rises rapidly and significantly compared to changes in ion temperature so the influence of ion conductivity can be ignored in the

modulation process. Changes of electron temperature during "heating-cooling" process act on electron density $N_e$, collision frequency between electrons and neutral particles $\upsilon_{en}$, eventually, it causes periodical variation of conductivity so that oscillating current is generated (Pashin et al., 1995):

$$|\Delta J| = \frac{1}{2}\left(1+\left(\frac{\Sigma_H}{\Sigma_P}\right)^2\right)^{1/2} \Delta\Sigma E_0 \tag{3.4}$$

$\Sigma_P$ and $\Sigma_H$ are the height-integrated Pedersen and Hall conductivity respectively. $\Delta\Sigma = \left((\Delta\Sigma_H)^2 + (\Delta\Sigma_P)^2\right)^{1/2}$, where $\Delta\Sigma_H$ and $\Delta\Sigma_P$ are disturbances of $\Sigma_H$ and $\Sigma_P$. It is worth noting that our model is based on the modulation of auroral electrojet, therefore the Cowling conductivity which is unique to the equatorial region is out of consideration in this thesis.

The magnetic field intensity of ELF/VLF waves received from the ground is (Pashin et al., 1995):

$$\Delta B = \frac{\mu_0}{4\pi}\frac{S}{z^2}|\Delta J| \tag{3.5}$$

Where $S$ is the horizontal cross-sectional area of the disturbed region. $z$ is the distance from the disturbed region to the receiver on the ground, $\mu_0$ is the permeability of free space.

### 3.1.2 Numerical simulation

In this part, we verified the validity of our physical model by comparing our simulation results with Cohen et al. (2010a). The chosen experiment (Cohen et al., 2010a) was conducted on 16 March 2008, 1300 UT, location is 62.4°N, 145.2°W (HAARP). The parameters of the ionosphere and atmosphere are obtained from IRI-2016 and NRLMSISE-00. The parameters of HF waves were 2.75 MHz, 420 MW, X wave. The modulation frequencies were from 2.5 kHz to 8.3 kHz, the duty cycle was 50%. The time step is $1\,\mu s$, the height range is 65~120 km with a spatial

resolution of 1 km. The $f_oE$ is only 0.36 MHz, which means this is an underdense heating process.

Figure 3.1 is the disturbance of electron temperature at all heights as a function of time when the modulation frequency is 2.5 kHz. It can be seen from the figure that the disturbance of electron temperature mainly occurs in the D region at a height of 80~90 km. Moreover, the response time is very short, which means that the electron temperature increases rapidly during the "heating" period and decreases rapidly during the "cooling" period, although the response time gradually increases with height, that is, the electron temperature at a higher height cannot reach steady-states in time during the heating and cooling stages. This phenomenon of insufficient heating and cooling becomes more obvious with the increase of the modulation frequency (i.e. the heating and cooling cycle is further shortened), and it is also an important reason that the intensity of stimulated ELF/VLF waves by conductivity modulation gradually decreases with the increase of frequency.

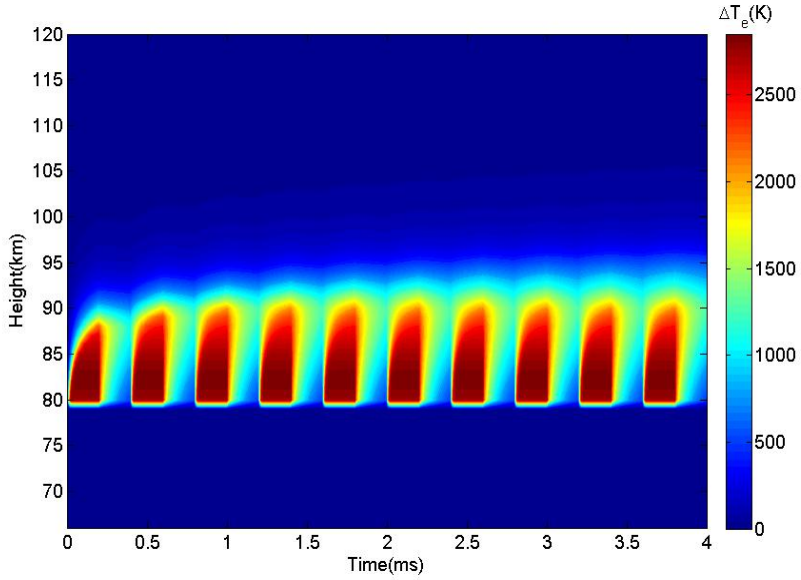


Figure 3.1 The disturbance of electron temperature at all heights varies over time during amplitude modulation for 10 times when the modulated frequency is 2.5 kHz with a 50% duty cycle.

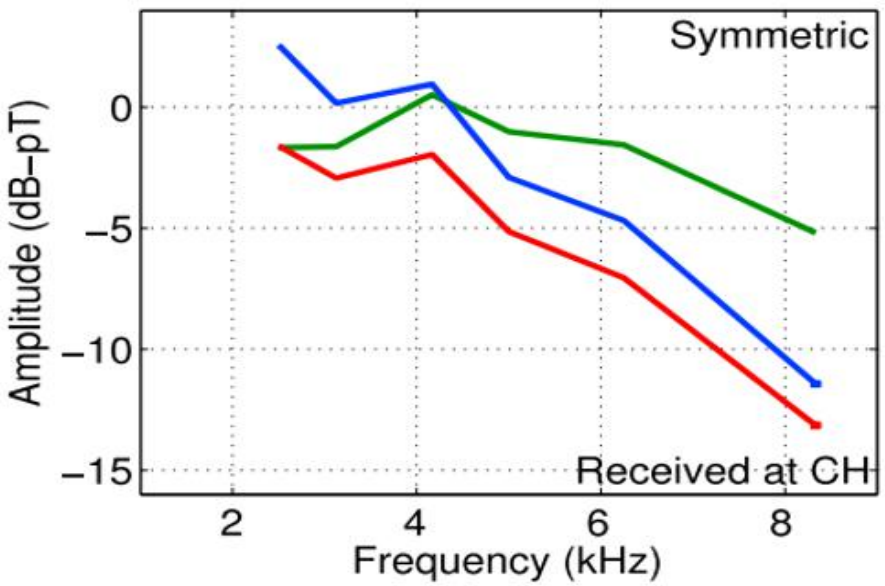


Figure 3.2 The ELF/VLF signal amplitude observed at Chistochina (62.62°N, −144.62°W, 37 km from HAARP) for amplitude modulation (red), beam painting (blue) and geometric modulation (green), "symmetric", referred to here as "vertical AM"(from Cohen et al., 2010a).

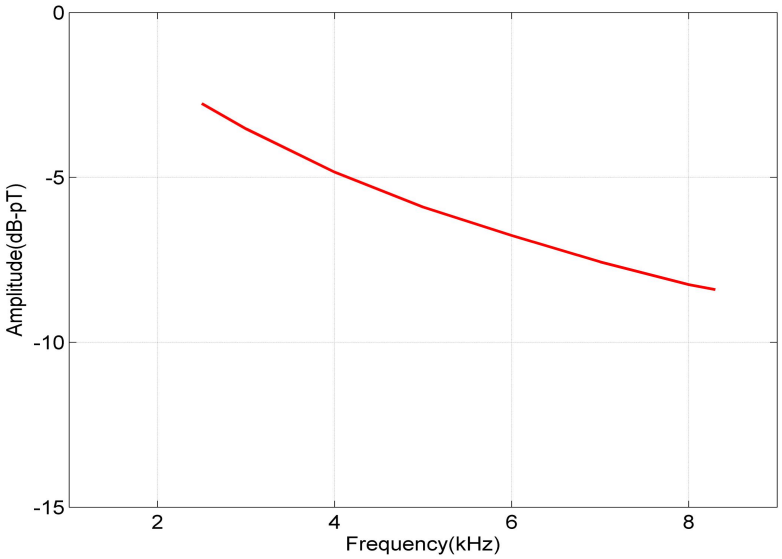


Figure 3.3 Our simulation results of the ELF/VLF signal amplitude observed at Chistochina for vertical amplitude modulation (the red line in Figure 3.2).

Figure 3.2 and 3.3 are the ELF/VLF signal observed on the ground (Cohen et al.,

2010a) and our corresponding simulation respectively. As can be seen from the figures, the efficiency of AM gradually decreases with the increase of the modulation frequency. Our simulation results are in good agreement with Cohen et al. (2010a) in the range of modulation frequency less than 6 kHz but larger than Cohen et al. (2010a) in the range above 6 kHz. We speculate that this may be due to the deviation between IRI-2016 and NRLMSISE-00 model and the real background ionosphere and atmosphere, which leads to a larger calculation result of the loss term in the energy equation, and makes the electron temperature to drop more significantly than the actual situation in the cooling stage.

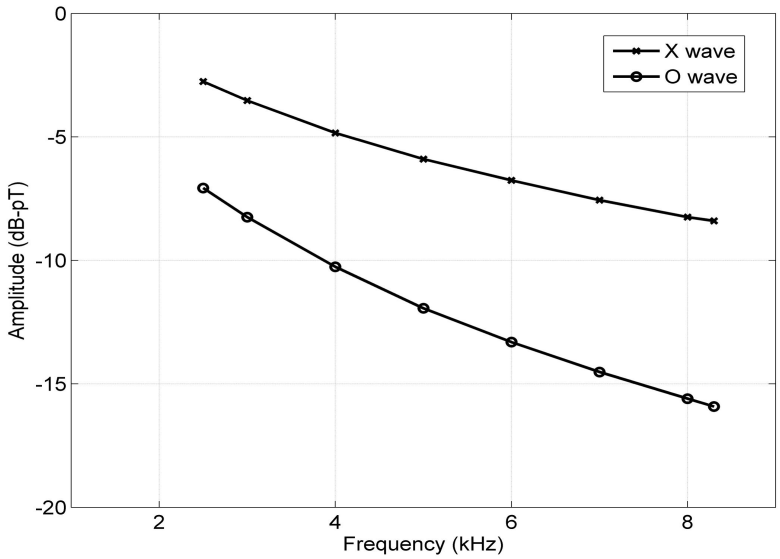


Figure 3.4 Numerical simulation of the ELF/VLF signal amplitude observed at Chistochina for X wave and O wave amplitude modulation with the modulated frequency varies from 2.5 kHz to 8.3 kHz.

Figure 3.4 is the comparison of modulation efficiency of X wave and O wave under the same background conditions (16 March 2008, 1300 UT, HAARP) and the HF wave parameters (2.75 MHz, 420 MW). As shown in the figure above, X wave is more efficient than O wave for amplitude modulation at all modulation frequencies. This is because the electron temperature enhancement in the D region is more efficient by X wave than by O wave.

## 3.2 Beat-wave Modulation

### 3.2.1 Physical model

Beat wave modulation is a modulation technique which transmits two high frequency continuous waves with frequencies $f_1 = f_0$ and $f_2 = f_0 + f$ respectively to stimulate ELF/VLF waves with frequency $f$. There are still controversies about the source region and mechanism of ELF/VLF waves generated by BW. Therefore, two theories about the mechanism of BW were introduced in this part: 1) based on the theory of electrojet modulation and 2) based on the theory of ponderomotive force. The first theory is essentially the same as AM and we just need to calculate the change of the power of HF waves during the beat wave process (Barr and Stubbe, 1997). Therefore, we mainly introduce the second theory - BW based on the ponderomotive force (Kuo et al., 2011). Simulations have been performed for each theory of beat wave modulation and compared with references.

The nonlinear beating current density at the beat frequency of the two HF waves is given by (Kuo et al., 2011):

$$\mathbf{J_B} = -\left(\frac{e}{\Omega_e}\right) \times \left\langle \nabla \cdot \left( N_e \mathbf{V_{pe}} \mathbf{V_{pe}} \right) \right\rangle \tag{3.6}$$

where $\Omega_e$ is the electron gyrofrequency, $\mathbf{V_{pe}}$ is the electron velocity induced by the HF heater, $N_e$ is the electron density, $\langle\ \rangle$ represents a VLF bandpass filter.

During the beat wave modulation process, the heater is split into two sub-arrays, transmitting continuous waves with a frequency difference in the ELF/VLF range, the frequency difference is the beat wave frequency. The electric field of the total HF heater is given by (Kuo et al., 2011):

$$\begin{aligned} \mathbf{E_p} &= \mathbf{E_{p1}} + \mathbf{E_{p2}} \\ &= (\pm \mathrm{i}\hat{\mathbf{y}}) \mathrm{E}_{\mathrm{p0}} [1 + \cos(\omega t - \psi)] \cos(k_0 z - \omega_0 t) \end{aligned} \tag{3.7}$$

where " ± " represent O waves and X waves respectively. $\mathrm{E}_{\mathrm{p0}}$ is the amplitude of each sub-array. $\omega = 2\pi f$ , $\psi$ is the phase difference between the radiations of the sub-arrays. $\omega_0$ and $k_0$ are the heater radian frequency and wave number respectively. Electron velocity induced by the heater is given by (Kuo et al., 2011):

$$\mathbf{V_{pe}} = -\mathrm{i}(\pm \mathrm{i}\hat{\mathbf{y}})\left[\left(e\mathrm{E}_{\mathrm{p0}}/m_e\right)/\left(\omega_0 \pm \Omega_e\right)\right]\cdot\left[1+\cos(\omega t-\psi)\right]\cos\left(k_0 z-\omega_0 t\right) \tag{3.8}$$

$m_e$ is the mass of electron.

Substituting equation (3.8) into equation (3.6), (3.6) becomes (Kuo et al., 2011):

$$\begin{aligned}\mathbf{J_B}(\mathbf{r},\mathrm{t}) &= \left(e/\Omega_e\right)\left[\left(e/m_e\right)/\left(\omega_0 \pm \Omega_e\right)\right]^2\left(\partial_x+\partial_y\right)\left(N_e\mathrm{E}_{\mathrm{p0}}^2\right)\cos\left(\omega t-\psi\right)\\ &= \mathbf{J}(\mathbf{r})\cdot 2\cos(\omega t)\end{aligned} \tag{3.9}$$

Where $\mathbf{J}(\mathbf{r}) = \left(e/2\Omega_e\right)\left[\left(e/m_e\right)/\left(\omega_0 \pm \Omega_e\right)\right]^2\left(\partial_x+\partial_y\right)\left(N_e\mathrm{E}_{\mathrm{p0}}^2\right)\cos\psi$ , " ± " represent O waves and X waves, respectively, the beating currents generated by X waves and O waves have a ratio proportional to $\left[\left(\omega_0+\Omega_e\right)/\left(\omega_0-\Omega_e\right)\right]^2$ , which means X waves are more effective to generate the beat wave current than O waves. Modeling (3.9) as a localized time harmonic current source with a gain factor *G* accounting for the finite size of the current distribution as well as the guiding effect of the geomagnetic field on the VLF wave propagation, then the phasor function $\mathbf{A}(\mathbf{r})$ of the vector potential of the ELF/VLF radiation is given by (Jackson, 1962 cited by Kuo et al., 2011):

$$\mathbf{A}(\mathbf{r}) = \left(\mathrm{e}^{\mathrm{i}kr}/r\right)G\int \mu_0\mathbf{J}\left(\mathbf{r}'\right)\mathrm{dV}' \tag{3.10}$$

Where $k$ is the wave number of the ELF/VLF wave, $\mu_0$ is the permeability of free space.

Finally, the magnetic field of the ELF/VLF radiation is given by (Kuo et al., 2011):

$$\mathbf{B}(\mathbf{r},t) = \nabla\times\mathbf{A}(\mathbf{r})\cdot 2\cos(\omega t) \tag{3.11}$$

## 3.2.2 Numerical simulation

### 3.2.2.1 Based on the theory of electrojet modulation

The validity of our physical model was verified by comparing our simulation results with Li et al. (2016). The result for comparison with our simulation is that of 20 November 2014, 1200 LT, the location of the heating site is 69.6°N, 19.2°E (Tromsø, EISCAT). The parameters of background ionosphere and atmosphere are from IRI-2016 and NRLMSISE-00 model respectively. The parameters of the HF wave are 1.16 GW ERP, X wave. The frequencies of these two continuous waves are $f_1 = f_0$ and $f_2 = f_0 + f$ where $f_0 = 4.1\,\mathrm{MHz}$ with modulation frequencies $f$ from 1 to 10 kHz. It is worth noting that the parameters of the heater above are not the real parameters of EISCAT, actually, they are the parameters of HAARP. This is because Li et al. (2016) want to show the possible results of BW at EISCAT if the heater of EISCAT has the same performance as HAARP. The time step is $1\,\mu\mathrm{s}$, the height range is 65~120 km with a spatial resolution of 1 km. The $f_oE$ is 1.48 MHz, which means this is an underdense heating process.

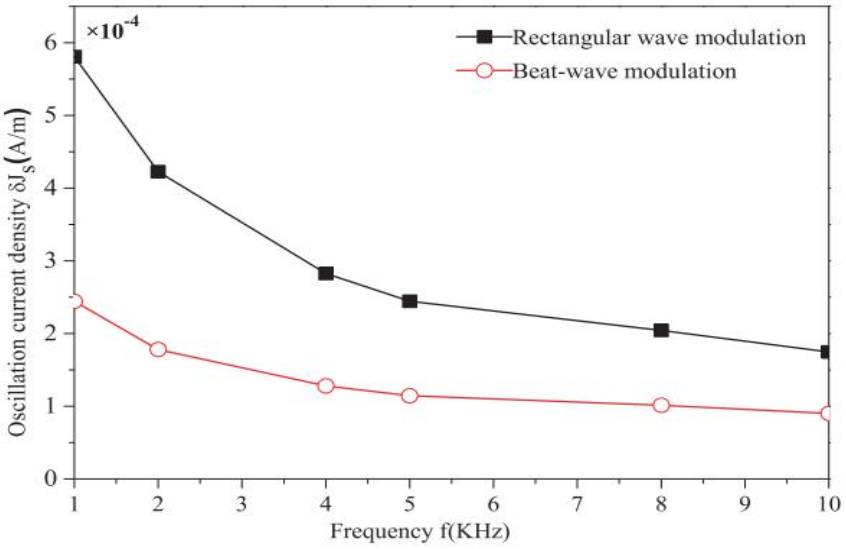


Figure 3.5 Oscillating current magnitudes of both rectangular wave modulation (AM) and beat-wave modulation when modulated frequency varies from 1 kHz to 10 kHz (from Li et al., 2016).

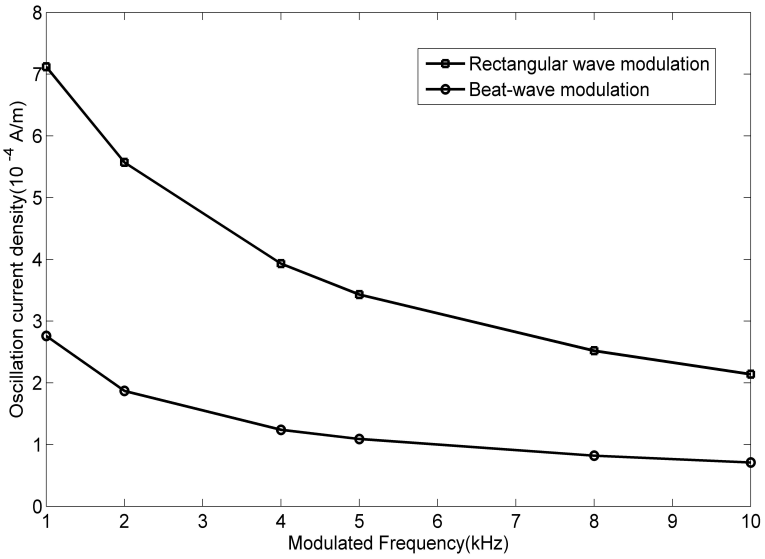


Figure 3.6 Our simulation results of oscillating current magnitudes modulated by rectangular wave modulation (AM) and beat wave modulation when modulated frequency varies from 1 kHz to 10 kHz with the same parameters as Li et al. (2016).

By comparing our simulation results (Figure 3.6) with Li et al. (2016) (Figure 3.5), we noticed that just like AM, BW based on electrojet modulation has the property that the modulation efficiency decreases with the increase of modulation frequency, in addition, AM is more effective than BW under the same conditions which is also consistent with the conclusions reached by Villaseñor (1996) and Barr and Stubbe (1997) through experiments. In short, our model is valid.

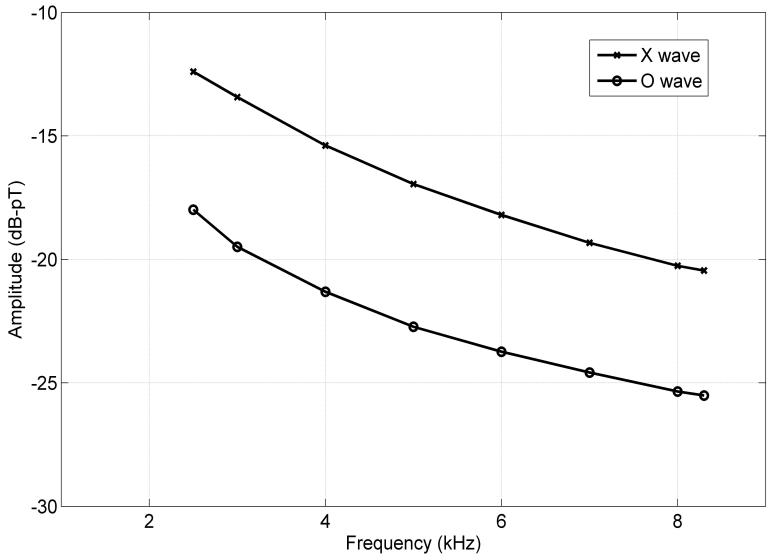


Figure 3.7 Numerical simulation of the ELF/VLF signal amplitude generated by beat wave modulation of X wave and O wave with the same ionospheric parameters (16 March 2008, 1300 UT, HAARP) and HF waves (2.75 MHz, 420 MW) as in section 3.1.2

In order to compare the efficiency of beat wave modulation by X wave and O wave, we took the same parameters of the ionosphere (16 March 2008, 1300 UT, HAARP) and HF waves (2.75 MHz, 420 MW) as in section 3.1.2 to make beat wave modulation with X and O wave, respectively. As shown in Figure 3.7, the efficiency of both X and O wave modulation decrease with the modulation frequency increasing and the amplitudes of ELF/VLF waves modulated by X wave are ~5 dB-pT greater than by O wave at all frequencies. In addition, by comparing Figure 3.7 with Figure 3.4, we noticed that the AM is indeed more efficient (~10-12 dB-pT greater) than BW.

#### 3.2.2.2 Based on the theory of ponderomotive force

In this part, we compared our simulation results with Kuo et al. (2011) to verify the validity of our physical model, also a comparison of the efficiency between BW and AM is made under the same conditions of ionospheric background and HF waves. The experiment (Kuo et al., 2011) chose was conducted on 4 April 2010, 0800 UT, at the

location of 62.4°N, 145.2°W (HAARP). The parameters of background ionosphere and atmosphere are from IRI-2016 and NRLMSISE-00 model respectively. HF waves were transmitted by the HAARP transmitter facility at full power (3.6 MW), where $f_0 = 3.2$ MHz with modulation frequencies $f = 5, 8, 13$ kHz. The time step is 0.1 ms, the height range is 120~400 km with a spatial resolution of 10 km × 10 km. The $f_oF2$ is 3.7 MHz, which means this is an overdense heating process. In addition, in order to verify the inference that X wave modulation is more effective than O wave modulation in equation (3.9), X wave and O wave are used for beat wave modulation, respectively.

Figure 3.8 and Figure 3.9 are the radiation amplitude received on the ground (Kuo et al., 2011) and our corresponding simulation results, respectively. It can be seen from the figures that in contrast to the theory of BW based on electrojet modulation, the efficiency of beat wave modulation based on ponderomotive force increases with the increase of the modulation frequency. Moreover, as indicated in equation (3.9), X wave is much more efficient than O wave for beat wave modulation. Our simulation results are generally in good agreement with Kuo et al. (2011).

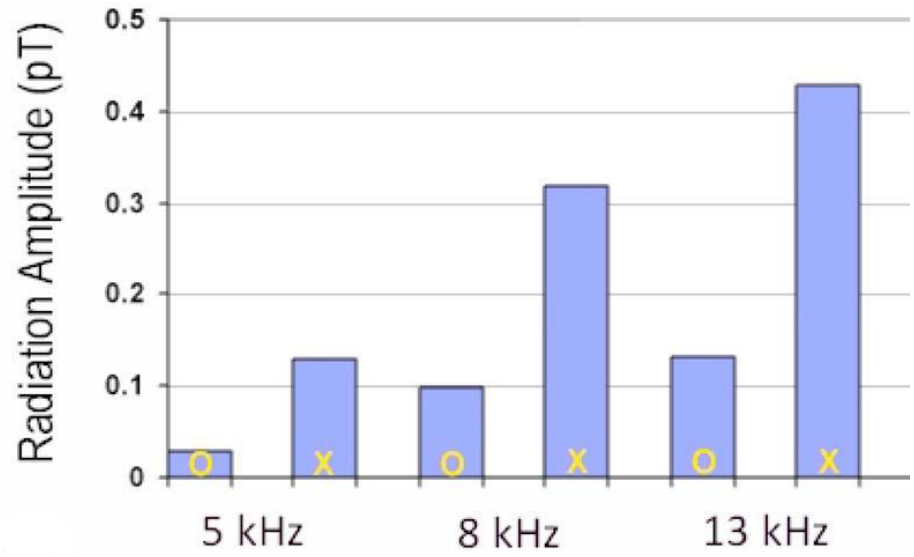


Figure 3.8 The averaged radiation amplitudes of VLF waves at several modulated frequencies (5 kHz, 8 kHz, 13 kHz) generated by the O and X wave beat wave modulation (from Kuo et al., 2011)

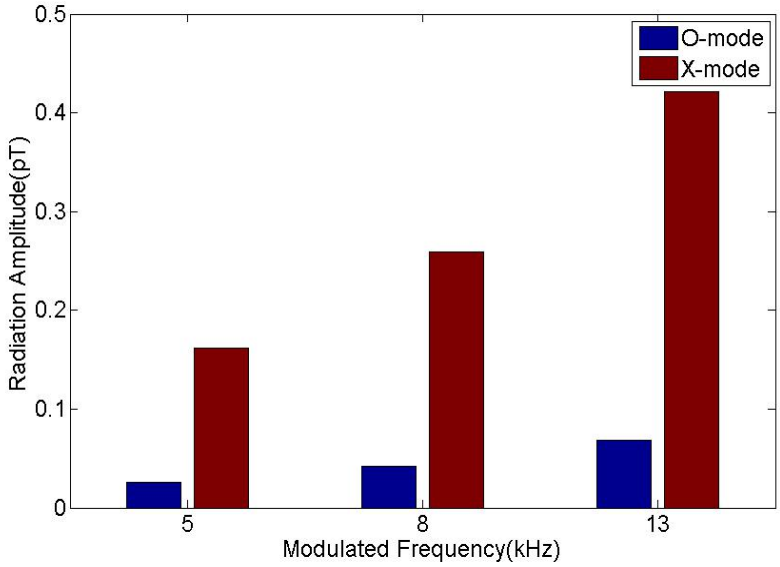


Figure 3.9 Our simulation results of the radiation amplitudes of VLF waves at several modulated frequencies (5 kHz, 8 kHz, 13 kHz) generated by the O and X wave beat wave modulation with the same parameters as Kuo et al. (2011).

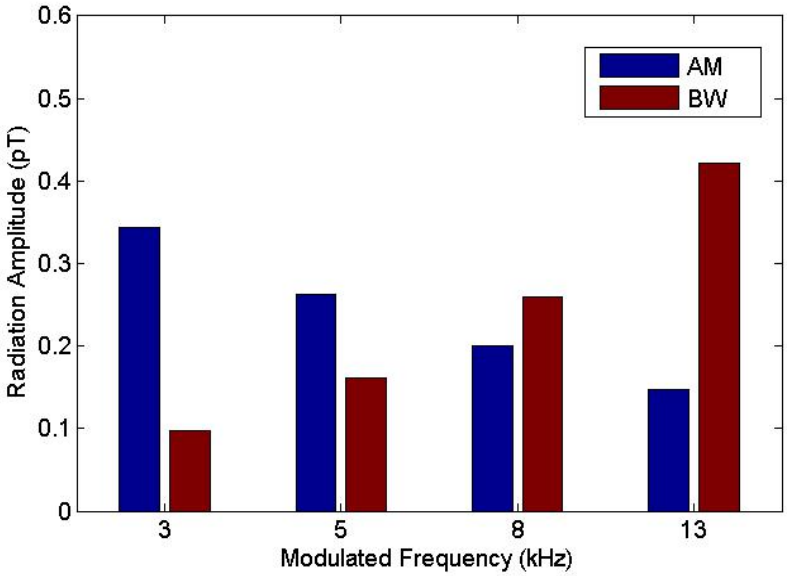


Figure 3.10 Numerical simulation of radiation amplitude of ELF/VLF waves at several modulated frequencies (3 kHz, 5 kHz, 8 kHz, 13 kHz) generated by amplitude modulation and beat wave modulation with the same parameters of ionosphere (4 April 2010, 0800 UT, HAARP) and HF waves (3.2 MHz, 570 MW, X wave).

In order to compare the efficiency of AM and BW, we took the same ionospheric parameters as those reported for the experiment on 4 April 2010, 0800 UT, at HAARP facility and HF waves (3.2 MHz, 570 MW, X wave) to make beat wave modulation and amplitude modulation, respectively. The results are shown in the Figure 3.10. The efficiency of AM decreases with an increase in the modulation frequency, while the efficiency of BW increases with an increase in modulation frequency. AM is more effective than BW when the modulation frequency is lower than 5~8 kHz, and BW is more effective than AM when the modulation frequency is higher than 5~8 kHz, which means BW is more suitable for VLF modulation with higher frequency, this conclusion is consistent with Cohen et al. (2012) and Kuo et al. (2012).

## 3.3 Summary

Our simulations results indicate that:

1) The modulation efficiency of AM and BW based on electrojet modulation has the same variation trend with the modulation frequency, that is, they both decrease with increasing the modulation frequency, and that AM is more effective than BW for ELF/VLF waves modulation at each modulation frequency.

2) The modulation efficiency of BW based on ponderomotive force and AM is quite opposite with regard to the modulation frequency. That is, the efficiency of BW based on ponderomotive force increases with the increase in modulation frequency. Therefore, AM is more suitable for ELF/VLF waves modulation at lower frequencies, while BW is more suitable for VLF waves modulation at higher frequencies.

3) The modulation efficiency of X wave is higher than that of O wave whether it is AM, BW based on electrojet modulation or BW based on ponderomotive force.

In summary, it can be seen that the two different theories of BW have different or even

completely opposite effect on the variation trend of the modulation efficiency with the modulation frequency. Therefore, we can conclude that both BW theories are valid but their efficiencies change with the modulation frequency. In fact, some scholars who support the theory of BW based on electrojet modulation (Cohen et al., 2012) and others who support the theory of BW based on ponderomotive force (Kuo et al., 2011) have also indicated that the possible effect of another theory cannot be completely ruled out. Therefore, in the next Chapter, we propose a new method to identify the mechanism of BW and the source region of ELF/VLF waves excitation.

# Chapter 4

# Identification of Mechanism and Source of BW

In Chapter 3, two different theories of BW with different or even completely opposite conclusions with regard to the variation trend of the modulation efficiency with the modulation frequency were introduced. According to the theory of BW based on electrojet modulation, the modulation efficiency decreases with an increase in the modulation frequency, whereas, the theory of BW based on ponderomotive force, results in an increase in the modulation efficiency when the modulation frequency is increased. In addition, these two theories correspond to different source regions of generating ELF/VLF waves. On the other hand, the variation trend of BW efficiency with modulation frequency is not always obvious as shown in Figure 1.10. Furthermore, some scholars who support the theory of BW based on electrojet modulation (Cohen et al., 2012) and others who support the theory of BW based on ponderomotive nonlinearity (Kuo et al., 2011) have also indicated that the possible effect of another theory cannot be completely ruled out, so in some cases the experimental results may be the effect of the combination of both of these two mechanisms. The main purpose of this Chapter is to propose a new method based on preheating technique to determine the mechanism of BW, or to determine the dominant or more important one when both mechanisms may be acting simultaneously.

## 4.1 Introduction of preheating

Preheating is a modulated heating technique proposed by Milikh and Papadopoulos (2007), which is essentially a method to change the background ionospheric parameters and thus affect the modulation efficiency by carrying out ionospheric heating before modulated heating. As shown in their simulations, a preheating of the lower ionosphere by a long HF-pulse (more than 500 s) can increase the peak intensity of the ELF/VLF signal by up to 7 dB. The physical mechanism of preheating is the same as the lower ionospheric heating introduced in Chapter 2, the key of its effect on modulated heating is that the electron density in the lower ionosphere increases after a period of preheating, which will affect the modulated heating in two aspects, firstly, for the electrojet modulation in D region, the increase of background electron density will increase the conductivity during the modulated heating process so that the modulation efficiency can be improved; secondly, for the BW based on the ponderomotive nonlinearity in F region, since there is no study at this point, we speculate on the possible results and then verify them in this Chapter. The “enhanced” D region after preheating will improve the D region absorption effect, which means the energy of HF waves actually reaching the F region will be further reduced, and therefore the modulation efficiency will be reduced as well. To sum up, since BW based on different physical mechanisms and source region positions have different responses to the preheating process, we believe that preheating may be a useful method to distinguish the physical mechanism and source region of BW.

## 4.2 Introduction of D region absorption

D region absorption can severely limit HF heating of the upper ionosphere, what’s more, this effect is hard to be offset by simply increasing the effective radiated power of the transmitted HF waves because the D region absorption also increases with heating power (Tomko et al., 1980). Tomko et al. (1980) found that in the case with an

obvious D region, at 100 km the attenuation of wave energy by self-absorption is about 3 dB for 100 MW of ionospheric heating and if one doubles the heating power to 200 MW, the self-absorption attenuation rises to more than 5 dB, which means that the remaining energy is less than 30%.

## 4.3 Numerical Simulation

### 4.3.1 D region absorption

The experiment (Yang et al., 2019b) carried out on December 4, 2018 at Tromsø, EISCAT is chosen as an example to illustrate the importance of D region absorption to BW in the F region. Figure 4.1 (a) and (b) are the profile of the background ionospheric electron density on 1000 UT and 1210 UT respectively (Yang et al., 2019b). The main difference of these two figures is that there is a strong D-E region in 1000 UT but the ionization of the lower ionosphere weakens and the D layer disappears in 1210 UT, which reduces the absorption attenuation of HF waves in the lower ionosphere. Therefore, the background plasma profiles in these two periods represent if D region absorption exists or not.

Table 4.1 shows the comparison of simulation results with experimental observations when carrying out beat wave modulation in the presence and absence of D region absorption. The frequency and ERP of transmitted HF waves are 4.04 MHz and 170 MW respectively, the modulation frequency is 2017 Hz. The receiver is located at 69.737°N, 18.896°E, about 15 km east of the EISCAT heating facility. It can be seen that there is a strong D region absorption at 1000 UT, so the ELF signal amplitude observed in the experiment is much smaller than the simulation results when we ignore the D region absorption effect. However, the simulation results are very close to the experimental observation results when we take the attenuation of wave energy caused by D layer absorption into consideration. In addition, the attenuation of wave energy in the lower ionosphere does not need to be considered at 1210 UT because the

ionization of the lower ionosphere weakens and the D region disappears, the simulation results are in good agreement with the experimental results.

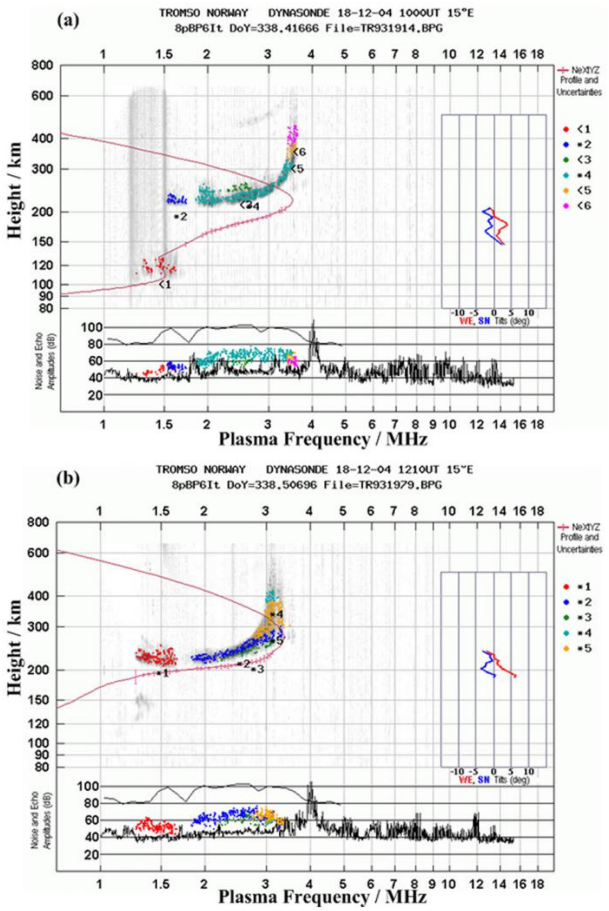


Figure 4.1 Status of the ionosphere during the experiments on December 4, 2018, 1000 UT (a) and 1210 UT (b) at Tromsø, EISCAT (from Yang et al., 2019b)

| Time | Existence of D region absorption | Observed amplitude (dBfT) | Simulation results ignoring D region absorption (dBfT) | Simulation results with D region absorption (dBfT) |
|---|---|---|---|---|
| 1000 UT | Yes | 18-21 | 26.3 | 21.2 |
| 1210 UT | No | 22-25 | 24.6 | 24.6 |

Table 4.1 Comparison of simulation results with experimental observations

## 4.3.2 Impact of preheating on BW

### 4.3.2.1 BW in D region

Firstly, the impact of preheating on BW based on electrojet modulation was simulated. In this case, the source region of generating ELF/VLF waves was located in the D region. Parameters of background ionosphere and atmosphere were consistent with section 3.1.2 (16 March 2008, 1300 UT, HAARP) which were obtained by IRI-2016 and NRLMSISE-00. The frequency, ERP and mode of HF waves were 2.75 MHz, 420 MW and X mode, respectively. The preheating wave was 4 MHz, 100 MW, X wave, and the duration of preheating was 5 s. For such a short time of preheating, the effect of preheating will last for just a few seconds. However, the time required for the electron density in the lower ionosphere to reach a stable state during ionospheric heating is usually tens of seconds, so a longer period of preheating means a more noticeable and long-lasting effect.

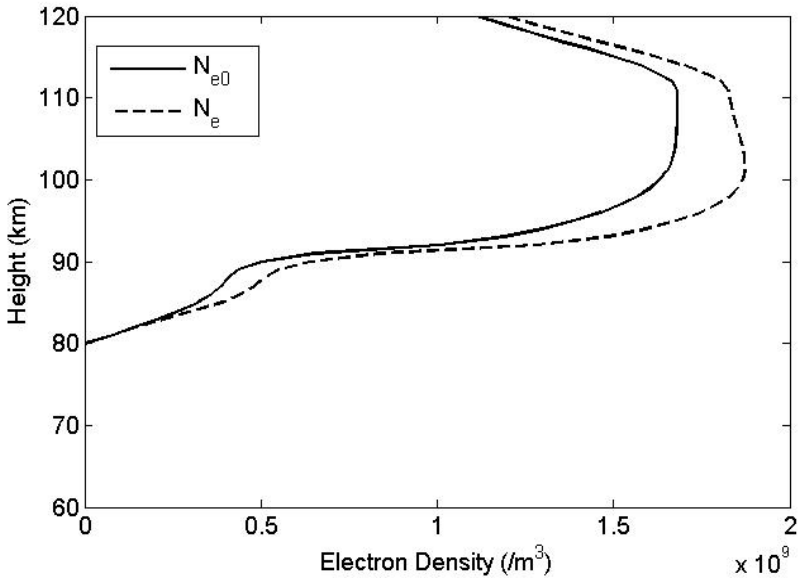


Figure 4.2 Profile of electron density before (solid line) and after (dashed line) preheating on 16 March 2008, 1300 UT, HAARP.

The solid and dashed lines in Figure 4.2 represent the profile of electron density before and after preheating, respectively. It can be seen from the figure that the electron density in the D and E region above 80 km increases significantly after

preheating for 5 s. According to equations (3.2), (3.3) and (3.4), an increase in background electron density can cause an increase in the conductivity and disturbance of current density. For the modulation frequency of 2000 Hz, the variations of current density disturbance for BW modulation before and after preheating were simulated as shown in Figure 4.3. When disturbances were basically stable, the disturbance of electric current density modulated by BW after preheating floated around $1.18\times10^{-4}$ A/m , while the disturbance of electric current density modulated by BW without preheating floated around $1.06\times10^{-4}$ A/m , which means that the preheating process indeed increases the disturbance of current density modulated by BW.

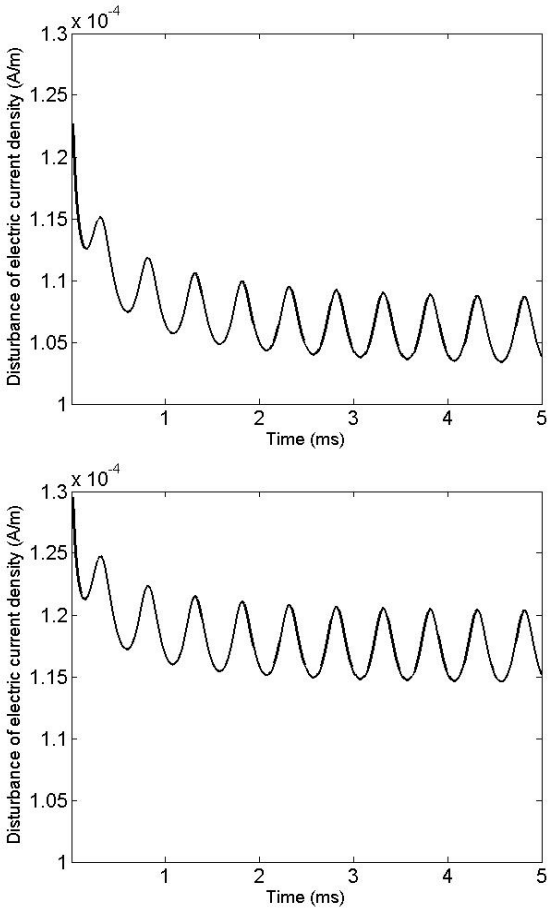


Figure 4.3 Disturbances of electric current density over time during BW with a modulated frequency $f = 2000\,\text{Hz}$ without (top) and after (bottom) preheating.

Finally, the signal amplitude of ELF waves obtained by receivers on the ground can be calculated using equation (3.5). In this case, the receiver is located at Chistochina

(62.62°N, −144.62°W, 37 km from HAARP). The same method was used to calculate the effect of preheating on the signal amplitude of ELF/VLF waves when the modulated frequencies were 3 kHz and 4 kHz, and the results are shown in Figure 4.4.

It can be seen from Figure 4.4 that although the modulation efficiency of BW after preheating still decreases with the increase of the modulated frequency which is a characteristic of electrojet modulation, preheating can increase the modulation efficiency at all modulated frequencies.

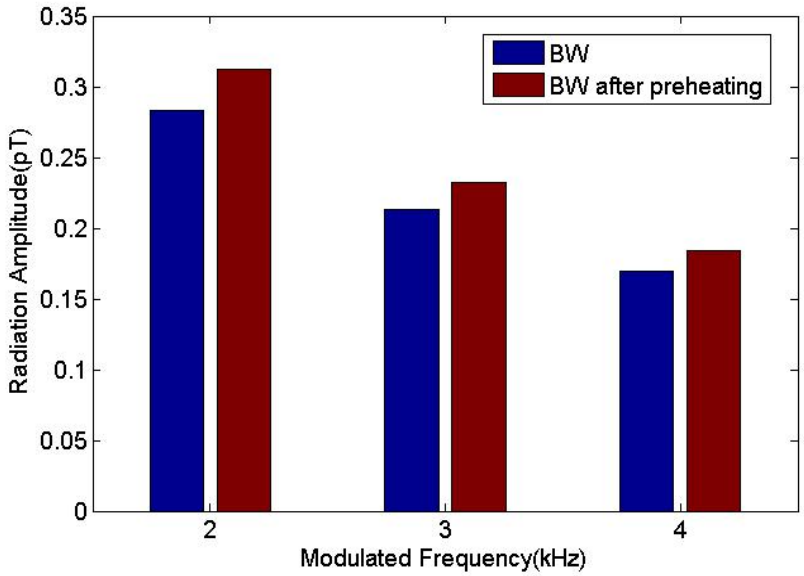


Figure 4.4 Simulation of signal amplitude of ELF/VLF waves generated by BW in D region with and without preheating at different modulated frequencies received at Chistochina (62.62°N, −144.62°W, 37 km from HAARP).

#### 4.3.2.2 BW in F region

The impact of preheating on BW based on ponderomotive nonlinearity is explored in this section. In this case, it is assumed that the source region of generating ELF/VLF waves was located in the F region. Background parameters of the ionosphere and atmosphere were the same as in section 4.3.1 (4 December 2018 1000 UT, Tromsø, EISCAT). Parameters of HF waves for modulated heating were 4.04 MHz, 170 MW, and X wave. Parameters of HF waves for preheating were 4 MHz, 100 MW, and X

wave, which were the same as in section 4.3.2.1, the duration of preheating was 5 s. As is mentioned above, the effect of preheating will last for a few seconds.

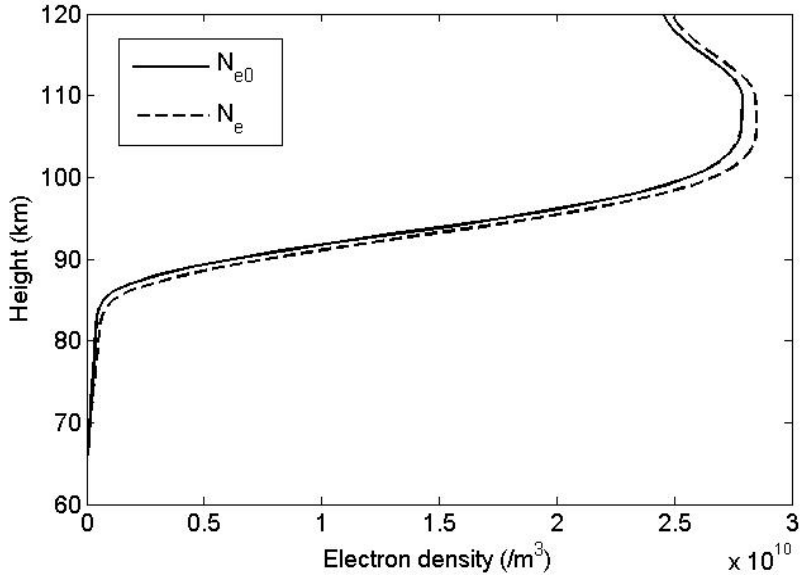


Figure 4.5 Profile of electron density before (solid line) and after (dashed line) preheating on 4 December 2018, 1000 UT, EISCAT

The solid and dashed lines in Figure 4.5 represent the profile of electron density before and after preheating, respectively. It can be seen from the figure that the electron density in the D and E region increases after preheating for 5 s.

It can be seen from Figure 4.6 that the power density of HF waves is reduced by D region absorption significantly. The “Initial” represents the background field without any heating process. According to calculation, when carrying out beat wave modulation without preheating, the power density drops to 52.4% of its initial value at the height of 120 km. In addition, the D region absorption effect becomes stronger after preheating, the power density for beat wave modulation after preheating for 5 s at the height of 120 km is only 42.9% of its initial value.

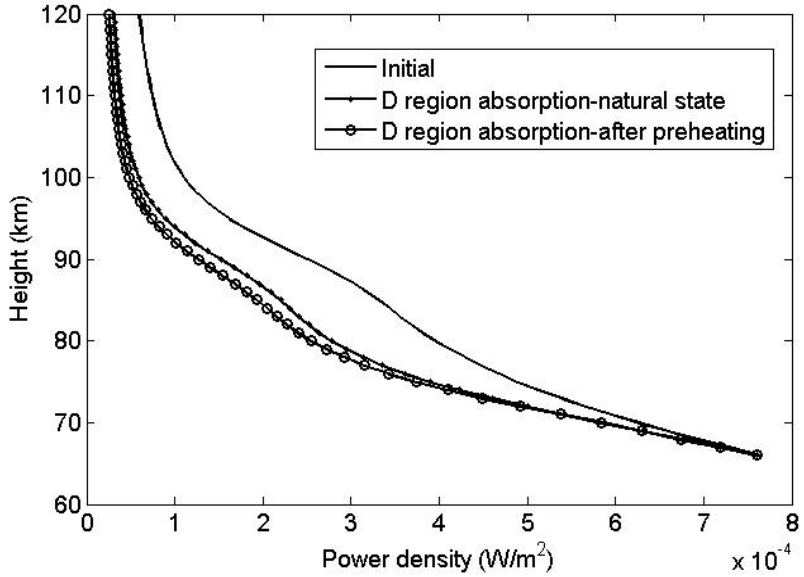


Figure 4.6 Power density of BW HF waves as a function of height. "Initial" represents the power density change with height at the start of the experiment without any heating process; "D region absorption - natural state" represents the power density change with height when carrying out beat wave modulation; "D region absorption - after preheating" represents the power density change with height when carrying out beat wave modulation after preheating for 5 s.

According to calculation, signal amplitudes of ELF/VLF waves (received at 69.737°N, 18.896°E, about 15 km east of EISCAT) generated by BW in F region and BW in F region after preheating with modulated frequencies at 2 kHz, 3 kHz, 4 kHz are shown on Figure 4.7. Preheating does not change the characteristic of the modulation efficiency of BW in the F region. The efficiency increases with the increase of the modulated frequency, but the modulation efficiency is reduced for all modulated frequencies compared with the case of no preheating.

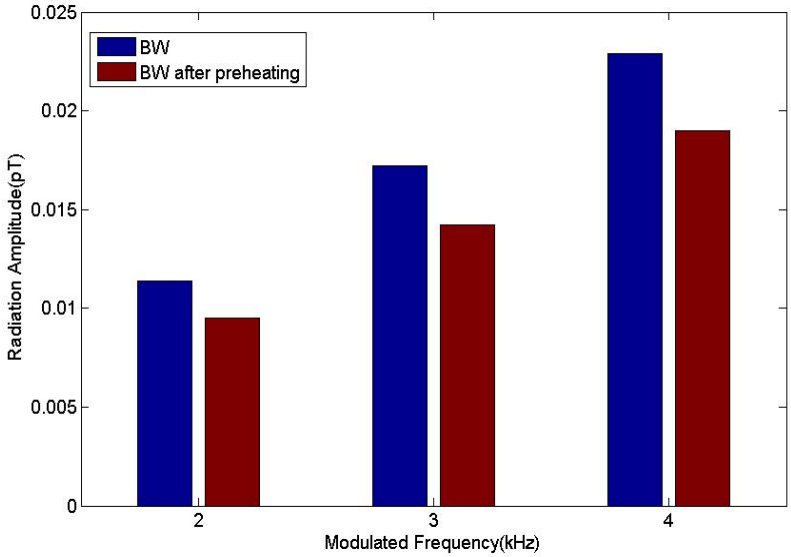


Figure 4.7 Simulation of signal amplitude of ELF/VLF waves generated by BW in F region with and without preheating at different modulated frequencies received at 69.737°N, 18.896°E, about 15 km east of EISCAT.

## 4.4 Summary

Our research in this Chapter indicated that:

1) When there are strong D and E regions in the ionosphere, the beat wave modulation in the F region will be affected by the strong D region absorption effect, the efficiency of beat wave modulation in the F region will be far lower than expected because of the attenuation of wave energy in the lower ionosphere.

2) The background electron density is increased in the lower ionosphere when preheated for a period of time, which leads to increased conductivity and modulated current density, as a result, the modulation efficiency of beat wave modulation in the D region is improved. The modulation efficiency of beat wave modulation in the D region after preheating still keeps the characteristic of decreasing with the increase of the modulated frequency, but in general, the modulation efficiency at all frequencies can be improved by preheating when compared with that without preheating.

3) In the presence of D and E regions in the ionosphere, the lower ionosphere can be further strengthened by preheating, which means greater impact of D region absorption on BW in the F region. As a result, less wave energy is transmitted to F region and therefore the modulation efficiency is reduced. Preheating does not change the characteristic that the modulation efficiency of BW in the F region increases with the increase of the modulated frequency, but the modulation efficiency at all frequencies is weakened by preheating when compared with the case without preheating.

To sum up, as the preheating process has opposite influence and effect on the efficiency of BW in the D region and F region, we believe that it can be used as a new method to judge the physical mechanism and source region of BW. However, it still needs to be tested and verified by experiments.

# Chapter 5

# Summary and Prospect

## 5.1 Summary

In this dissertation, the main mechanisms of ionospheric heating as well as amplitude modulation and beat wave modulation in both D and F regions have been considered. Physical models for D and F region heating were constructed and simulations based on these physical models were made to compare with published work so that the validity of our physical models can be verified; finally, a possible method based on preheating technique has been proposed to identify the mechanism and the source region of beat wave modulation.

### 5.1.1 Modeling of ionospheric heating as well as AM and BW

The increase of electron temperature during ionospheric heating is mainly due to the Ohmic heating effect. It is essentially the collision and absorption of high frequency waves by particles in the ionosphere. The changes of electron temperature and density are the main effects of Ohmic heating. This process can be expressed by three basic equations (energy equation, dynamic equation and continuity equation). However, because of the differences in plasma parameters and physical processes at different ionospheric regions, the basic equations in the lower and upper ionosphere are slightly different. As a result, physical models of lower ionospheric heating and upper ionospheric heating were constructed separately.

The physical model of ionospheric heating was extended to include modulated heating for AM and BW, respectively. The substance of AM is electrojet modulation based on thermal nonlinearity so that the source region of modulated ELF/VLF waves is located in the D region. However, the mechanism of BW is controversial; this dissertation aims to shed light on this controversy, by constructing physical models for BW in the D region based on thermal nonlinearity and BW in the F region based on ponderomotive nonlinearity, respectively.

### 5.1.2 Simulation of ionospheric heating and modulated heating

Comparisons of our simulations with those published in the literature illustrates the validity of our physical models of ionospheric heating and modulated heating. The simulation results reported in this dissertation indicate that:

1) The change of electron density is negligible for modulated heating in both lower and higher ionospheric altitudes.

2) Both AM and BW in the D region decrease with increasing the modulation frequency, and that AM is more effective than BW in the D region for ELF/VLF waves modulation at each modulation frequency.

3) The efficiency of BW based on ponderomotive force increases with increasing the modulation frequency, in contrast to the case of AM. In addition, AM is more suitable for ELF/VLF waves modulation at lower frequencies, while BW is more suitable for VLF waves modulation at higher frequencies.

4) The modulation efficiency of X wave is higher than that of O wave whether it is AM, BW based on electrojet modulation or BW based on ponderomotive force.

### 5.1.3 Identification of the mechanism and source region of beat wave modulation by preheating

According to our simulation results and some references, these two different theories of BW have different or even completely opposite conclusions on the variation trend of the modulation efficiency with the modulated frequency. In addition, some experiments show the variation trend of BW efficiency with modulated frequency may be irregular (Ma et al., 2019). Therefore, considering that BW in different regions may react differently to the same external disturbance such as preheating, it is proposed to consider preheating as a way to distinguish and identify the source region of BW.

According to simulation, it is found that:

1) BW in the F region can be affected by D region absorption, as a result, the efficiency of BW in the F region can be far lower than expected because of the attenuation of wave energy by D region absorption.

2) The D region can be "strengthened" by preheating which means D region absorption can be strengthened simultaneously. Finally, the modulation efficiency of BW in the F region at all frequencies can be weakened by preheating when compared with that without preheating.

3) The modulation efficiency of BW in the D region at all frequencies can be improved by preheating when compared with that without preheating because of the positive role of preheating on ionospheric conductivity.

4) Preheating will not change the trend of modulation efficiency of either BW in the D region or BW in the F region with modulated frequency.

To sum up, because of the opposite impact of preheating on the efficiency of BW in D

and F regions, preheating is proposed as a possible method to identify the physical mechanism and source region of BW.

## 5.2 Prospect

There are three aspects in which this research can be extended further:

1) BW in the D region and F region are simulated separately based on current models. However, the actual situation may be more complicated, that is, both the D region and F region play a role in BW. Therefore, further research can be carried out by building a physical model including BW in the D region and F region simultaneously. In this case, preheating may be useful to obtain more meaningful results for determining whether the D region or F region plays a more important role in BW under different initial conditions, that is, we need to find out the dominant source region of BW and the reason for this.

2) At present, the simulation study of preheating to identify the mechanism of BW has not been verified by experiments. Therefore，the design of proving experiment is also a key point of further research as part of my Ph.D. work.

3) Further experiments carried out at middle latitude will be very useful for identifying the mechanism and source region of BW because of the lack of electrojet in the ionosphere.

# Bibliography

Agrawal, D., & Moore, R. C. (2012). Dual-beam ELF wave generation as a function of power, frequency, modulation waveform, and receiver location. *Journal of Geophysical Research: Space Physics*, 117(A12), A12305, doi:10.1029/2012ja018061

Allen, E. M., Thome, G. D., & Rao, P. B. (1974). HF phased array observations of heater-induced spread-F. *Radio Science, 9(11), 905–916.* doi:10.1029/rs009i011p00-905

Bailey, V. A. (1937a). Resonance in the Interaction of Radio Waves. *Nature, 139(3524), 838–839.* doi:10.1038/139838a0

Bailey, V. A. (1937b). On some effects caused in the ionosphere by electric waves. *Phil. Mag*, 23(157), 929. https://doi.org/10.1080/14786443708561867

Bailey, V. A., & Goldstein, L. (1958). Control of the ionosphere by means of radio waves. *Journal of Atmospheric and Terrestrial Physics*, 12(2-3), 216–217. doi:10.1016/0021-9169(58)90094-1

Barr, R. & Stubbe, P. (1997). ELF and VLF wave generation by HF heating: A comparison of AM and CW techniques. *Journal of Atmospheric and Solar-Terrestrial Physics*, 59(18), 2265–2279. doi:10.1016/s1364-6826(96)00121-6

Barr, R. (1996). VLF wave generation using VLF heating and the cubic nonlinearity of the ionosphere. *Geophysical Research Letters, 23(16), 2165–2168.* doi:10.1029/96gl02024

Barr, R. (1997). VLF wave generation using VLF heating: a pointer to a new technique for ELF wave production? *IEE Proceedings - Microwaves, Antennas and Propagation, 144(3), 153.* doi:10.1049/ip-map:19971196

Barr, R., Rietveld, M. T., Stubbe, P., & Kopka, H. (1987). Ionospheric heater beam scanning: A mobile source of ELF radiation. *Radio Science*, 22(6), 1073–1083. doi:10.1029/rs022i006p01073

Barr, R., Rietveld, M. T., Stubbe, P., & Kopka, H. (1988). Ionospheric heater beam scanning: A realistic model of this mobile source of ELF/VLF radiation. *Radio Science, 23(3), 379–388.* doi:10.1029/rs023i003p00379

Barr, R., Stubbe, P., & Rietveld, M. T. (1999). ELF wave generation in the ionosphere using pulse modulated HF heating: initial tests of a technique for increasing ELF wave generation efficiency. *Annales Geophysicae*, 17(6), 759-769. https://doi.org/10.1007/s00585-999-0759-0

Belenov, A. F., Erukhimov, L. M., Ponomarenko, P. V., & Yampolski, Y. M. (1997). Interaction between artificial ionospheric turbulence and geomagnetic pulsations. *Journal of Atmospheric and Solar-Terrestrial Physics, 59(18), 2367–2372.* doi:10.1016/s1364-6826(96)00130-7

Bernhardt, P. & Duncan, L. (1982). The feedback-diffraction theory of ionospheric heating. *Journal of Atmospheric and Terrestrial Physics, 44(12), 1061–1074.* doi:10.1016/0021-9169(82)90018-6

Bernhardt, P. A., Duncan, L. M., & Tepley, C. A. (1989). Heater-induced cavities as optical tracers of plasma drifts. *Journal of Geophysical Research: Space Physics, 94(A6), 7003–7010.* doi:10.1029/ja094ia06p07003

Blagoveshchenskaya, N. F., Borisova, T. D., Yeoman, T. K., Rietveld, M. T., Ivanova, I. M., & Baddeley, L. J. (2011). Artificial small-scale field-aligned irregularities in the

high latitude F region of the ionosphere induced by an X-mode HF heater wave. *Geophysical Research Letters, 38(8),* (L08), 802. doi:10.1029/2011gl046724

Blagoveshchenskaya, N. F., Borisova, T. D., Yeoman, T. K., Rietveld, M. T., Häggström, I., & Ivanova, I. M. (2013). Plasma modifications induced by an X-mode HF heater wave in the high latitude F region of the ionosphere. *Journal of Atmospheric and Solar-Terrestrial Physics, 105-106, 231-244.* doi:10.1016/j.jastp. 2012.10.001

Blaunstein, N. (1996). Changes of the electron concentration profile during local heating of the ionospheric plasma. *Journal of Atmospheric and Terrestrial Physics, 58(12), 1345–1354.* doi:10.1016/0021-9169(95)00160-3

Carpenter, D. L. (2002). Small-scale field-aligned plasmaspheric density structures inferred from the Radio Plasma Imager on IMAGE. *Journal of Geophysical Research, 107(A9).* doi:10.1029/2001ja009199

Cohen, M. B., & Gołkowski, M. (2013). 100 days of ELF/VLF generation via HF heating with HAARP. *Journal of Geophysical Research: Space Physics*, 118(10), 6597–6607. doi:10.1002/jgra.50558

Cohen, M. B., Golkowski, M., Lehtinen, N. G., Inan, U. S., & McCarrick, M. J. (2012). HF beam parameters in ELF/VLF wave generation via modulated heating of the ionosphere. *Journal of Geophysical Research: Space Physics*, 117(A5), A05327. doi:10.1029/2012ja017585

Cohen, M. B., Inan, U. S., & Gołkowski, M. (2009). Reply to comment by R. C. Moore and M. T. Rietveld on "Geometric modulation: A more effective method of steerable ELF/VLF wave generation with continuous HF heating of the lower ionosphere." *Geophysical Research Letters,* 36(4). doi:10.1029/2008gl036519

Cohen, M. B., Inan, U. S., & Golkowski, M. A. (2008). Geometric modulation: A

more effective method of steerable ELF/VLF wave generation with continuous HF heating of the lower ionosphere. *Geophysical Research Letters*, 35(12), L12101. doi:10.1029/2008gl034061

Cohen, M. B., Inan, U. S., Gołkowski, M. & McCarrick, M. J. (2010a), ELF/VLF wave generation via ionospheric HF heating: Experimental comparison of amplitude modulation, beam painting, and geometric modulation, *J. Geophys. Res.*, 115, A02302, doi:10.1029/2009JA014410

Cohen, M. B., Inan, U. S., Gołkowski, M., & Lehtinen, N. G. (2010b). On the generation of ELF/VLF waves for long-distance propagation via steerable HF heating of the lower ionosphere. *Journal of Geophysical Research: Space Physics*, 115(A7). doi:10.1029/2009ja015170

Cohen, M. B., Moore, R. C., Golkowski, M. & Lehtinen, N. G. (2012). ELF/VLF wave generation from the beating of two HF ionospheric heating sources. *Journal of Geophysical Research: Space Physics*, 117(A12), A12310. doi:10.1029/2012ja018140

De Soria-Santacruz, M., Bautista, G., Gettliffe, G. V., Martinez-Sanchez, M., & Miller, D. W. (2014). Design of a space-borne antenna for controlled removal of energetic Van Allen belt protons. *2014 IEEE Aerospace Conference.* doi:10.1109/aero. 2014.6836244

Djuth, F. T., Sulzer, M. P., & Elder, J. H. (1990). High resolution observations of HF-induced plasma waves in the ionosphere. *Geophysical Research Letters*, 17(11), 1893–1896. doi:10.1029/gl017i011p01893

DuBois, D. F., Rose, H. A., & Russell, D. (1990). Excitation of strong Langmuir turbulence in plasmas near critical density: Application to HF heating of the ionosphere. *Journal of Geophysical Research*, 95(A12), 21221. doi:10.1029/ja-095ia12p21221

Duncan, L. M., Sheerin, J. P., & Behnke, R. A. (1988). Observations of Ionospheric Cavities Generated by High-Power Radio Waves. *Physical Review Letters*, 61(2), 239–242. doi:10.1103/physrevlett.61.239

Eliasson, B., Chang, C.-L., & Papadopoulos, K. (2012). Generation of ELF and ULF electromagnetic waves by modulated heating of the ionospheric F2 region. *Journal of Geophysical Research: Space Physics*, 117(A10), A10320. doi:10.1029/2012ja017935

Fejer, J., Gonzales, C., Ierkic, H., Sulzer, M., Tepley, C., Duncan, L., … Gordon, W. (1985). Ionospheric modification experiments with the Arecibo Heating Facility. *Journal of Atmospheric and Terrestrial Physics*, 47(12), 1165–1179. doi:10.1016/0021-9169(85)90086-8

Ferraro, A. J., Lee, H. S., Allshouse, R., Carroll, K., Tomko, A. A., kelly, F. J., & Joiner, R. G. (1982). VLF/ELF radiation from the ionospheric dynamo current system modulated by powerful HF signals. *Journal of Atmospheric and Terrestrial Physics*, 44(12), 1113–1122. doi:10.1016/0021-9169(82)90022-8

Frolov, V. L., Erukhimov, L. M., Metelev, S. A., & Sergeev, E. N. (1997). Temporal behaviour of artificial small-scale ionospheric irregularities: Review of experimental results. *Journal of Atmospheric and Solar-Terrestrial Physics*, 59(18), 2317–2333. doi:10.1016/s1364-6826(96)00126-5

Frolov, V. L., Papoport, V. O., Komrakov, G. P., Belov, A. S., Markov, G. A., Parrot, M., … Mishin, E. V. (2008). Satellite measurements of plasma-density perturbations induced in the topside ionosphere by high-power HF radio waves from the “Sura” heating facility. *Radiophysics and Quantum Electronics*, 51(11), 825–833. doi:10.1007/s11141-009-9086-2

Fu, H. Y. (2017). *Ionospheric Heating Research by High Power HF Transmitters: Physics, Application and Progress*. In: China Research Institute of Radiowave Propagation, The 14th Chinese National Symposium on Radio Propagation. Qingdao,

September 14-16, 2017.

Fujimaru, S. & Moore, R. C. (2011). Analysis of time-of-arrival observations performed during ELF/VLF wave generation experiments at HAARP. *Radio Science*, 46(3), RS0M03. doi:10.1029/2011rs004695

Gekelman, W., Pribyl, P., Lucky, Z., Drandell, M., Leneman, D., Maggs, J., … DeHaas, T. (2016). The upgraded Large Plasma Device, a machine for studying frontier basic plasma physics. *Review of Scientific Instruments*, 87(2), 025105. doi:10.1063/1.4941079

Getmantsev, G. G., Zuikov, N. A., Kotik, D. S., Mironenko, L. F., Mitiakov, N. A., Rapoport, V. O., ... & Eidman, V. I. (1974). Combination frequencies in the interaction between high-power short-wave radiation and ionospheric plasma. *Sov. Phys. JETP, Engl. Transl.*, 20, 229-232.

Gigliotti, A., Gekelman, W., Pribyl, P., Vincena, S., Karavaev, A., Shao, X., … Papadopoulos, D. (2009). Generation of polarized shear Alfvén waves by a rotating magnetic field source. *Physics of Plasmas*, 16(9), 092106. doi:10.1063/1.3224030

Ginzburg, V. L., & Gurevich, A. V. (1960). *NONLINEAR PHENOMENA IN A PLASMA LOCATED IN AN ALTERNATING ELECTROMAGNETIC FIELD. Soviet Physics Uspekhi*, 3(1), 115–146. doi:10.1070/pu1960v003n01abeh003261

Gołkowski, M., Cohen, M. B., & Moore, R. C. (2013). Modulation of auroral electrojet currents using dual modulated HF beams with ELF phase offset, a potential D-region ionospheric diagnostic. *Journal of Geophysical Research: Space Physics*, 118(5), 2350–2358. doi:10.1002/jgra.50230

Gołkowski, M., Inan, U. S., & Cohen, M. B. (2009). Cross modulation of whistler mode and HF waves above the HAARP ionospheric heater. *Geophysical Research Letters*, 36(15), L15103. doi:10.1029/2009gl039669

Gurevich, A. V. (2007). Nonlinear effects in the ionosphere. *Physics-Uspekhi*, 50(11), 1091–1121. doi:10.1070/pu2007v050n11abeh006212.

Hansen, J. D., Morales, G. J., & Maggs, J. E. (1992). Large-scale HF-induced ionospheric modifications: Theory and modeling. *Journal of Geophysical Research*, 97(A11), 17019. doi:10.1029/92ja01603

Helliwell, R. A. (1988). VLF wave stimulation experiments in the magnetosphere from Siple Station, Antarctica. *Reviews of Geophysics*, 26(3), 551. doi:10.1029/rg-026i003p00551

Hinkel-Lipsker, D. E., Shoucri, M. M., Smith, T. M., Wagner, T. M., Hansen, J. D., & Morales, G. J. (1993). Modeling of high-frequency oblique propagation and heating in the ionosphere. *Radio Science*, 28(5), 819–837. doi:10.1029/93rs01578

Huang, W. G. & Gu, S. F. (2003a). Interaction between the powerful high-frequency radio wave and the lower terrestrial ionosphere. *Chinese Journal of Space Science*, 23(3), 181-188. doi: 10.11728/cjss2003.03.181. (in Chinese)

Huang, W. G. & Gu, S. F. (2003b). The heating of upper ionosphere by powerful high-frequency radio waves. *Chinese Journal of Space Science*, 23(5), 343-351. doi:10.3969/j.issn.0254-6124.2003.05.004. (in Chinese)

Huang, W. G., Gu, S. F., & Gong, J. C. (2004). Ionospheric heating by powerful high-frequency radio waves. *Chinese Journal of Radio Science*, 19(3), 296-301. doi:10.13443/j .c jors.2004.03.009. (in Chinese)

Huba, J. D., Joyce, G., & Fedder, J. A. (2000). Sami2 is Another Model of the Ionosphere (SAMI2): A new low-latitude ionosphere model. *Journal of Geophysical Research: Space Physics*, 105(A10), 23035–23053. doi:10.1029/2000ja000035

Huba, J. D., Joyce, G., & Krall, J. (2008). Three-dimensional equatorial spread F

modeling. *Geophysical Research Letters*, 35(10). doi:10.1029/2008gl033509

Inan, U. S. (2004). Multi-hop whistler-mode ELF/VLF signals and triggered emissions excited by the HAARP HF heater. *Geophysical Research Letters*, 31(24). doi:10.1029/2004gl021647

Jin, G., M. Spasojevic, M. B. Cohen, U. S. Inan, & N. G. Lehtinen (2011). The relationship between geophysical conditions and ELF amplitude in modulated heating experiments at HAARP: Modeling and experimental results, *J. Geophys. Res.*, 116, A07310. doi:10.1029/2011JA016664

Jones, R. M., & Stephenson, J. J. (1975). *A versatile three-dimensional ray tracing computer program for radio waves in the ionosphere*. Washington, D.C.: U.S. Government Printing Office.

Karavaev, A. V., Gumerov, N. A., Papadopoulos, K., Shao, X., Sharma, A. S., Gekelman, W., ... & Vincena, S. (2011). Generation of shear Alfvén waves by a rotating magnetic field source: Three-dimensional simulations. *Physics of Plasmas*, 18(3), 032113. https://doi.org/10.1063/1.3562118

Karavaev, A. V., Gumerov, N. A., Papadopoulos, K., Shao, X., Sharma, A. S., Gekelman, W., … Vincena, S. (2010). Generation of whistler waves by a rotating magnetic field source. *Physics of Plasmas*, 17(1), 012102. doi:10.1063/1.3274916

Kosch, M. J., Rietveld, M. T., Hagfors, T., & Leyser, T. B. (2000). High-latitude HF-induced airglow displaced equatorwards of the pump beam. *Geophysical Research Letters*, 27(17), 2817 – 2820. doi:10.1029/2000gl003754

Kotik, D. S., & Ermakova, E. N. (1998). Resonances in the generation of electromagnetic signals due to the thermal cubic nonlinearity in the lower ionosphere. *Journal of Atmospheric and Solar-Terrestrial Physics*, 60(12), 1257-1259. doi:10.1016/s1364-6826(98)00053-4

Kuo, S. P., & Lee, M. C. (2017). On the VLF wave generation by beating of two HF heaters. *Physics of Plasmas*, 24(2), 022902. doi:10.1063/1.4976123

Kuo, S., Cheng, W.-T., Pradipta, R., Lee, M. C., & Snyder, A. (2013). Observation and theory of whistler wave generation by high-power HF waves. *Journal of Geophysical Research: Space Physics*, 118(3), 1331–1338. doi:10.1002/jgra.50193

Kuo, S., Snyder, A., & Chang, C.-L. (2010). Electrojet-independent ionospheric extremely low frequency/very low frequency wave generation by powerful high frequency waves. *Physics of Plasmas*, 17(8), 082904. doi:10.1063/1.3476290

Kuo, S., Snyder, A., Kossey, P., Chang, C.-L., & Labenski, J. (2012). Beating HF waves to generate VLF waves in the ionosphere. *Journal of Geophysical Research: Space Physics*, 117(A3), A03318. doi:10.1029/2011ja017076

Kuo, S., Snyder, A., Kossey, P., Chang, C.-L., & Labenski, J. (2011). VLF wave generation by beating of two HF waves in the ionosphere. *Geophysical Research Letters*, 38(10), L10608. doi:10.1029/2011gl047514

Li, B. (2006). *Preliminary theoretical research on artificial ionospheric Spread-F.* MSc. Wuhan University. (in Chinese)

Li, H.-Y., Zhan, J., Wu, Z.-S., & Kong, P. (2016). Numerical simulations of ELF/VLF wave generated by modulated beat-wave ionospheric heating in high latitude regions. *Progress In Electromagnetics Research M*, 50, 55–63. doi:10.2528/pierm16062604

Liu, L. , Wu, X., Tu, J., & Bao, Z. (1997). Modeling study of modification of the lower ionosphere by vlf electromagnetic waves. *Chinese Journal of Space Science,* 17(2), 130-135. (in Chinese)

Ma, G., Guo, L., Yang, J., Lv, L., Chen, J., Xu, T., … Wu, J. (2019). Effects of variations of geomagnetic field on VLF waves induced by beating of two HF waves.

*Advances in Space Research*, 63 (2019) 2126–2131. doi:10.1016/j.asr.2018.12.031

Martin, M. J., Pribyl, P., Gekelman, W., & Lucky, Z. (2015). An RF amplifier for ICRF studies in the LAPD. doi:10.1063/1.4936517

Maxworth, A. S., Gołkowski, M., Cohen, M. B., Moore, R. C., Chorsi, H. T., Gedney, S. D., & Jacobs, R. (2015). Multistation observations of the azimuth, polarization, and frequency dependence of ELF/VLF waves generated by electrojet modulation. *Radio Science*, 50(10), 1008–1026. doi:10.1002/2015rs005683

Meltz, G., Rush, C. M., & Violette, E. J. (1982). Simulation of D and E region high-power microwave heating with HF ionospheric modification experiments. *Radio Science*, 17(3), 701–715. doi:10.1029/rs017i003p00701

Milikh, G. M., & Papadopoulos, K. (2007). Enhanced ionospheric ELF/VLF generation efficiency by multiple timescale modulated heating. *Geophysical Research Letters*, 34(20). doi:10.1029/2007gl031518

Milikh, G. M., Demekhov, A. G., Papadopoulos, K., Vartanyan, A., Huba, J. D., & Joyce, G. (2010b). Model for artificial ionospheric duct formation due to HF heating. *Geophysical Research Letters*, 37(7), L07803. doi:10.1029/2010gl042684

Milikh, G. M., Demekhov, A., Vartanyan, A., Mishin, E. V., & Huba, J. (2012). A new model for formation of artificial ducts due to ionospheric HF-heating. *Geophysical Research Letters*, 39(10), L10102. doi:10.1029/2012gl051718

Milikh, G. M., Mishin, E., Galkin, I., Vartanyan, A., Roth, C., & Reinisch, B. W. (2010a). Ion outflows and artificial ducts in the topside ionosphere at HAARP. *Geophysical Research Letters*, 37(18), L18102. doi:10.1029/2010gl044636

Milikh, G. M., Papadopoulos, K., Shroff, H., Chang, C. L., Wallace, T., Mishin, E. V., … Berthelier, J. J. (2008). Formation of artificial ionospheric ducts. *Geophysical*

*Research Letters*, 35(17). doi:10.1029/2008gl034630

Moore, R. C., & Agrawal, D. (2011). ELF/VLF wave generation using simultaneous CW and modulated HF heating of the ionosphere. *Journal of Geophysical Research: Space Physics*, 116(A4), L04217. doi:10.1029/2010ja015902

Moore, R. C., & Rietveld, M. T. (2009). Comment on "Geometric modulation: A more effective method of steerable ELF/VLF wave generation with continuous HF heating of the lower ionosphere" by M. B. Cohen, U. S. Inan, and M. A. Golkowski. *Geophysical Research Letters*, 36(4). doi:10.1029/2008gl036002

Moore, R. C., Fujimaru, S., Cohen, M., Gołkowski, M., & McCarrick, M. J. (2012). On the altitude of the ELF/VLF source region generated during "beat-wave" HF heating experiments. *Geophysical Research Letters*, 39(18). doi:10.1029/2012-gl053210

Moore, R. C., Fujimaru, S., Kotovsky, D. A., & Gołkowski, M. (2013). Observations of Ionospheric ELF and VLF Wave Generation by Excitation of the Thermal Cubic Nonlinearity. *Physical Review Letters*, 111(23). doi:10.1103/physrevlett.111.235007

Moore, R. C., Inan, U. S., Bell, T. F., & Kennedy, E. J. (2007). ELF waves generated by modulated HF heating of the auroral electrojet and observed at a ground distance of ~4400 km. *Journal of Geophysical Research: Space Physics*, 112(A5), A05309. doi:10.1029/2006ja012063

Nagaraja, M., & Prasad, S. (2017). *Going Beyond Chu's Limit: ULF Radiation with Directly Modulated Spinning Magnet Arrays.* MSc. UCLA

Nishitani, N., Ruohoniemi, J. M., Lester, M., Baker, J. B. H., Koustov, A. V., Shepherd, S. G., ... & Marchaudon, A. (2019). Review of the accomplishments of mid-latitude Super Dual Auroral Radar Network (SuperDARN) HF radars. *Progress in Earth and Planetary Science*, 6(1), 1-57. doi: 10.1186/s40645-019-0270-5

Papadopoulos, K., Chang, C. L., Vitello, P., & Drobot, A. (1990). On the efficiency of ionospheric ELF generation. *Radio science*, 25(06), 1311-1320. doi: 10.1029/RS025i-006p01311

Papadopoulos, K., Chang, C., Labenski, J., Wallace, T., (2011a). First demonstration of HF-driven ionospheric currents. *Geophys. Res. Lett.*, 38 (L20), 107. http://dx.doi.org/10.1029/2011GL049263

Papadopoulos, K., Gumerov, N., Shao, X., Doxas, I., Chang, C., (2011b). HF-driven currents in the polar ionosphere. Geophys. *Res. Lett.*, 38 (L12), 103. http://dx.doi.org/10.1029/2011GL047368

Pashin, A. B., Belova, E. G., & Lyatsky, W. B. (1995). Magnetic pulsation generation by a powerful ground-based modulated HF radio transmitter. *Journal of Atmospheric and Terrestrial Physics*, 57(3), 245–252. doi:10.1016/0021-9169(93)e0005-t

Perrine, R. P., Milikh, G. M., Papadopoulos, K., Huba, J. D., Joyce, G., Swisdak, M., & Dimant, Y. (2006). An interhemispheric model of artificial ionospheric ducts. *Radio Science, 41(4), RS4002.* doi:10.1029/2005rs003371

Pedersen, T. R., & Carlson, H. C. (2001). First observations of HF heater-produced airglow at the High Frequency Active Auroral Research Program facility: Thermal excitation and spatial structuring. *Radio Science*, 36(5), 1013 – 1026. doi:10.1029/2000rs002399

Rietveld, M. T. (2003). Ionospheric electron heating, optical emissions, and striations induced by powerful HF radio waves at high latitudes: Aspect angle dependence. *Journal of Geophysical Research*, 108(A4). doi:10.1029/2002ja009543

Rietveld, M., Kopka, H. & Stubbe, P. (1986). D-region characteristics deduced from pulsed ionospheric heating under auroral electrojet conditions. *Journal of Atmospheric and Terrestrial Physics*, 48(4), 311–326. doi:10.1016/0021-9169(86)90001-2

Robinson, A., & Moore, R. C. (2017). Optimization of VLF/ELF Wave Generation using Beam Painting. *AGUFM 2017*, SM23B-2615

Rooker, L. A., Lee, M. C., Pradipta, R., & Watkins, B. J. (2013). Generation and detection of whistler wave induced space plasma turbulence at Gakona, Alaska. *Physica Scripta*, T155, 014029. doi:10.1088/0031-8949/2013/t155/014029

Sergienko, T., Gustavsson, B., Steen, Å., Brändström, U., Rietveld, M., Leyser, T. B., & Honary, F. (2000). Analysis of excitation of the 630.0 nm airglow during a heating experiment in Tromsø on February 16, 1999. *Physics and Chemistry of the Earth, Part B: Hydrology, Oceans and Atmosphere, 25(5-6), 531–535.* doi:10.1016/s1464-1909(00)00059-9

Sharma, A. S., Eliasson, B., Shao, X., & Papadopoulos, K. (2016). Generation of ELF waves during HF heating of the ionosphere at midlatitudes. *Radio Science*, 51(7), 962–971. doi:10.1002/2016rs005953

Streltsov, A. V., Berthelier, J.-J., Chernyshov, A. A., Frolov, V. L., Honary, F., Kosch, M. J., … Rietveld, M. T. (2018). Past, Present and Future of Active Radio Frequency Experiments in Space. *Space Science Reviews*, 214(8). doi:10.1007/s11214-018-0549-7

Streltsov, A. V., Guido, T., Tulegenov, B., Labenski, J., & Chang, C.-L. (2014). Artificial excitation of ELF waves with frequency of Schumann resonance. *Journal of Atmospheric and Solar-Terrestrial Physics*, 119, 110–115. doi:10.1016/j.jastp.-2014.07.004

Streltsov, A. V., Lampe, M., Manheimer, W., Ganguli, G., & Joyce, G. (2006). Whistler propagation in inhomogeneous plasma. *Journal of Geophysical Research*, 111(A3). doi:10.1029/2005ja011357

Stubbe, P., & Varnum, W. S. (1972). Electron energy transfer rates in the ionosphere.

*Planetary and Space Science*, 20(8), 1121–1126. doi:10.1016/0032-0633(72)90001-3

Stubbe, P., Kopka, H., Rietveld, M., Frey, A., Høeg, P., kohl, H., … Holt, O. (1985). Ionospheric modification experiments with the Tromsø heating facility. *Journal of Atmospheric and Terrestrial Physics*, 47(12), 1151–1163. doi:10.1016/0021-9169(85)90085-6

Tellegen, B. D. H. (1933). Interaction between radio-waves?. *Nature*, 131(3319), 840-840.

Tereshchenko, E. D., Shumilov, O. I., Kasatkina, E. A., & Gomonov, A. D. (2014). Features of amplitude and Doppler frequency variation of ELF/VLF waves generated by “beat-wave” HF heating at high latitudes. *Geophysical Research Letters*, 41(13), 4442–4448. doi:10.1002/2014gl060376

Thome, G. D., & Blood, D. W. (1974). First observations of RF backscatter from field-aligned irregularities produced by ionospheric heating. *Radio Science*, 9(11), 917–921. doi:10.1029/rs009i011p00917

Tomko, A. A., Ferraro, A. J. & Lee, H. S. (1980). D region absorption effects during high-power radio wave heating. *Radio Science*, 15(3), 675–682. doi:10.1029/rs015i-003p00675

Utlaut, W. F., & Cohen, R. (1971). Modifying the Ionosphere with Intense Radio Waves. *Science*, 174(4006), 245–254. doi:10.1126/science.174.4006.245

Utlaut, W. F., & Violette, E. J. (1972). Further ionosonde observations of ionospheric modification by a high-powered HF transmitter. *Journal of Geophysical Research*, 77(34), 6804–6818. doi:10.1029/ja077i034p06804

Vartanyan, A., Milikh, G. M., Eliasson, B., Najmi, A. C., Parrot, M., & Papadopoulos, K. (2016). Generation of whistler waves by continuous HF heating of the upper

ionosphere. *Radio Science*, 51(7), 1188–1198. doi:10.1002/2015rs005892

Villaseñor, J., Wong, A. Y., Song, B., Pau, J., McCarrick, M., & Sentman, D. (1996). Comparison of ELF/VLF generation modes in the ionosphere by the HIPAS heater array. *Radio Science*, 31(1), 211–226. doi:10.1029/95rs01993

Wang, J. S. & Lv, J. Y. (2012). *Space Weather*. Beijing: China Meteorological Press. (in Chinese)

Wang, Z. G., Xu, B., & Xu, Z. W. (2012). A comparison of numerical simulation and measurements during ionospheric heating. *Chinese J. Geophys*, 53(3), 751-759. doi: 10.6038/j.issn.0001-5733.2012.03.004 (in Chinese)

Weik, M. H. (2000a). left-hand circular polarization. *Computer Science and Communications Dictionary*, 883 – 883. doi:10.1007/1-4020-0613-6_10062

Weik, M. H. (2000b). right-hand circular polarization. *Computer Science and Communications Dictionary*, 1494 – 1494. doi:10.1007/1-4020-0613-6_16386

Willis, J. W., & Davis, J. R. (1973). Radio frequency heating effects on electron density in the lower E region. *Journal of Geophysical Research*, 78(25), 5710–5717. doi:10.1029/ja078i025p05710

Wu, T.-W., Huba, J. D., Joyce, G., & Bernhardt, P. A. (2012). Modeling Arecibo conjugate heating effects with SAMI2. *Geophysical Research Letters*, 39(7), L07103. doi:10.1029/2012gl051311

Xiong, N. L., Tang, C. C., Li, X. J. (1999). *Introduction to Ionospheric Physics*. Wuhan: Wuhan University Press. (in Chinese)

Xu, T., Rietveld, M., Wu, J., Ma, G., Hu, Y., Wu, J., & Li, Q. (2019). Polarization analysis of ELF/VLF waves generated by beating of two HF waves in the polar ionosphere. *Journal of Atmospheric and Solar-Terrestrial Physics*, 196, 105133.

doi:10.1016/j.jastp.2019.105133

Xu, X., Zhou, C., Shi, R., Ni, B., Zhao, Z., & Zhang, Y. (2016). Numerical study of the generation and propagation of ultralow-frequency waves by artificial ionospheric F region modulation at different latitudes. *Annales Geophysicae*, 34(9), 815–829. doi:10.5194/angeo-34-815-2016

Yang, J. T., Wang, J. G., Li Q. L., Che, H. Q. & Hao, S. J. (2019a). Optimized analysis of ionospheric amplitude modulated heating parameters for excitation of very/extremely low frequency radiations. *Plasma Science and Technology*, 21(7), 075301

Yang, J., Li, Q., Wang, J., Hao, S., & Ma, G. (2018). The polarization characteristics of ELF/VLF waves generated via HF heating experiments of the ionosphere by EISCAT. *Physics of Plasmas*, 25(9), 092902. doi:10.1063/1.5044611

Yang, J. T., Wang, J. G., Li, Q. L., Wu, J., Che, H. Q., Ma, G. L. & Hao, S. J. (2019b). Experimental comparisons between AM and BW modulation heating excitation of ELF/VLF waves at EISCAT. *Physics of Plasmas*, 26(8), 082901. https://doi.org/10.1063/1.5095537

Ye, G. & Liu, Z. (1983). *The theory of ionospheric waves*. Beijing: Science Press. (in Chinese)

Zawdie, K. A., Huba, J. D., & Wu, T.-W. (2013). Modeling 3-D artificial ionospheric ducts. *Journal of Geophysical Research: Space Physics*, 118(11), 7450–7457. doi:10.1002/2013ja018823

Zhou, C., Wang, X., Liu, M. et al. (2018). Nonlinear processes in ionosphere: Report on the mechanisms of ionospheric heating by the powerful radio waves. *Chinese Journal of Geophysics*, 61(11): 4323-4336, doi: 10.6038/cjg2018M0048. (in Chinese)